iScience

CellPress
OPEN ACCESS

Article

Epidermal Growth Factor Receptor Inhibition Reverses Cellular and Transcriptomic Alterations Induced by Hypoxia in the Neonatal Piglet Brain

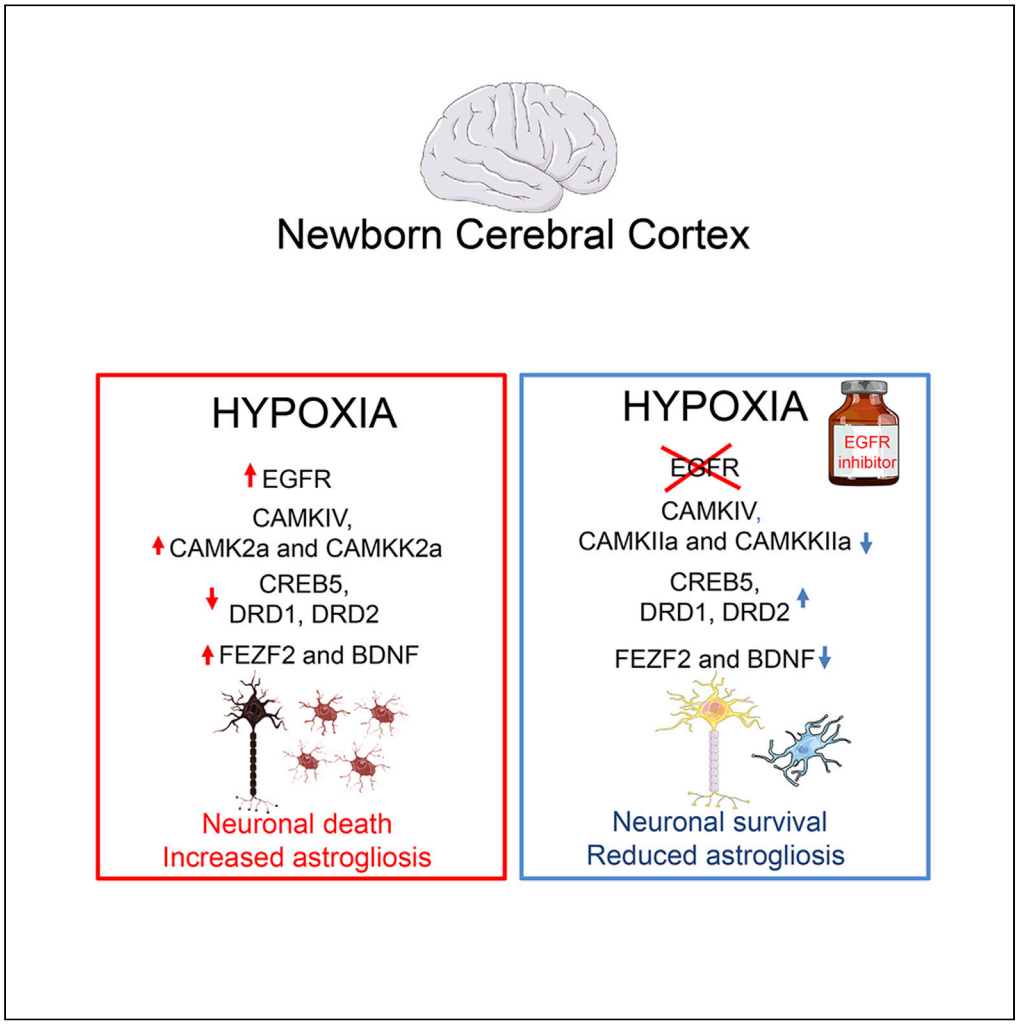

Panagiotis Kratimenos, Evan Z. Goldstein, Ioannis Koutroulis, ..., M. Isabel Almira-Suarez, Vittorio Gallo, Maria Delivoria-Papadopoulos

panagiotis.kratimenos@childrensnational.org (P.K.)
vgallo@childrensnational.org (V.G.)

HIGHLIGHTS

EGFR mediates the effects of neonatal hypoxia in piglet and human cerebral cortex

EGFR inhibition reverses pathological changes induced by hypoxia in piglet cortex

EGFR blockage prevents hypoxia-induced transcriptomic changes in piglet cortex

EGFR-associated pathways are therapeutic targets in neonatal hypoxic injury

Kratimenos et al., iScience 23, 101766
December 18, 2020
https://doi.org/10.1016/j.isci.2020.101766

iScience

CellPress
OPEN ACCESS

Article

Epidermal Growth Factor Receptor Inhibition Reverses Cellular and Transcriptomic Alterations Induced by Hypoxia in the Neonatal Piglet Brain

Panagiotis Kratimenos,[1,2,*] Evan Z. Goldstein,[1] Ioannis Koutroulis,[3,4,5] Susan Knoblach,[4,5] Beata Jablonska,[1] Payal Banerjee,[4] Shadi N. Malaeb,[6] Surajit Bhattacharya,[4] M. Isabel Almira-Suarez,[7] Vittorio Gallo,[1,9,*] and Maria Delivoria-Papadopoulos[6,8]

SUMMARY

Acute hypoxia (HX) causes extensive cellular damage in the developing human cerebral cortex. We found increased expression of activated-EGFR in affected cortical areas of neonates with HX and investigated its functional role in the piglet, which displays a highly evolved, gyrencephalic brain, with a human-like maturation pattern. In the piglet, HX-induced activation of EGFR and Ca^{2+}/calmodulin kinase IV (CaMKIV) caused cell death and pathological alterations in neurons and glia. EGFR blockade inhibited CaMKIV activation, attenuated neuronal loss, increased oligodendrocyte proliferation, and reversed HX-induced astrogliosis. We performed for the first time high-throughput transcriptomic analysis of the piglet cortex to define molecular responses to HX and to uncover genes specifically involved in EGFR signaling in piglet and human brain injury. Our results indicate that specific molecular responses modulated by EGFR may be targeted as a therapeutic strategy for HX injury in the neonatal brain.

INTRODUCTION

Hypoxic (HX) encephalopathy is the major cause of death and neurodevelopmental disability in newborns (Lawn et al., 2005; Kurinczuk et al., 2010). Decreased oxygen and energy failure in the brain led to neuronal cell death (Martin et al., 1997b; Mehmet et al., 1998; DiGiacomo et al., 1992), but the cellular and molecular mechanisms of HX-induced neuronal and glial cell damage are still largely undefined. Future cell-based therapeutic interventions depend on identifying specific signaling pathways and their selective role in the pathophysiology of HX, leading to long-term neurological sequelae.

Cell death signaling in the neonatal brain involves the apoptotic and the rat sarcoma/mitogen-activated protein kinase (Ras/MAPK) pathways (Chin et al., 1997; Hognason et al., 2001), and the initial HX insult linked to activation of these pathways causes oxygen free radical formation and lipid peroxidation of the neuronal membrane. We have previously shown that HX activates a set of apoptotic enzymes in the area of focal adhesions (FAs) and a variety of membrane receptors, including the epidermal growth factor receptor (EGFR) (Kratimenos et al., 2017b; Delivoria-Papadopoulou and Malaeb, 2014). Located at the cell membrane, the EGFR plays an essential role in cell growth and proliferation and has been shown to be neuroprotective following HX via nuclear factor (NF)-κB-dependent transcriptional upregulation of cyclin D1 (Chen et al., 2016). However, EGFR activation can also induce neural cell damage and apoptotic cell death (Armstrong et al., 1994; Jackson and Ceresa, 2017).

There is significant cross-interaction between different molecular elements of the FAs network, which ultimately result in either promoting cell proliferation and motility (mitogenic) or apoptotic cell death (Kratimenos et al., 2014, 2017c). It has been shown that EGFR overexpression induces apoptosis through molecular alterations of the glutamate ionotropic receptor N-methyl-D-aspartate (NMDA)-type subunit 2B (GluN2B) (Tang et al., 2015). Modification of the NMDA receptor by oxygen free radicals promotes calcium influx into the cytosol, deactivation of protein tyrosine phosphatases, and activation of EGFR kinase (Maulik et al., 2008; Vibert et al., 2008). This series of events causes downstream activation of nuclear CaMKIV, CREB

[1]Center for Neuroscience Research, Children's National Research Institute, Children's National Hospital, George Washington University School of Medicine and Health Sciences, 111 Michigan Avenue, NW, Washington, DC 20010 P 202-476-5922, USA

[2]Department of Pediatrics, Division of Neonatology, Children's National Hospital and George Washington University School of Medicine and Health Sciences, 111 Michigan Avenue, NW, Washington, DC 20010 P 202-602-4889, USA

[3]Department of Pediatrics, Division of Emergency Medicine, Children's National Hospital and George Washington University School of Medicine and Health Sciences, Washington, DC, USA

[4]Research Center for Genetic Medicine, Children's National Research Institute, Washington, DC, USA

[5]Department of Genomics and Precision Medicine, George Washington University School of Medicine and Health Sciences, Washington, DC, USA

[6]Department of Pediatrics, Drexel University College of Medicine, Philadelphia, PA, USA

[7]Department of Pathology, Children's National Hospital and George Washington University School of Medicine and Health Sciences, Washington, DC, USA

[8]Deceased author

[9]Lead Contact

*Correspondence: panagiotis.kratimenos@childrensnational.org (P.K.), vgallo@childrensnational.org (V.G.)

https://doi.org/10.1016/j.isci.2020.101766

transcription, and the formation of the apoptosome and caspase activation, ultimately leading to DNA fragmentation and cell death (Mishra et al., 2009, 2010).

The newborn piglet is a powerful model to study human brain development, as it displays a highly evolved, gyrencephalic brain (Ishibashi et al., 2012; Imai et al., 2006). Furthermore, cortical development and anatomical structure are similar in piglet and human, and—like in human—approximately 50% of the piglet brain volume is represented by white matter (Felix et al., 1999; Imai et al., 2006). The similar white/gray matter ratio and developmental age at term with human brain (Thoresen et al., 1996; Haaland et al., 1997; Bjorkman et al., 2006; Odden et al., 1989; Jain et al., 2017; Martin et al., 1997a, 1997b; Brambrink et al., 1999; Guerguerian et al., 2002; Ezzati et al., 2017; Groenendaal et al., 1999; Mehmet et al., 1994, 1998; Yue et al., 1997) make the piglet an ideal preclinical model to study the cellular and developmental consequences of neonatal brain injury, including HX, and potential therapeutic interventions. Finally as the piglet shares many metabolic and physiological similarities with humans, the effects of pharmacological treatment in pigs resemble those in humans more closely than other laboratory animals (Forster et al., 2010).

In the present study, we first performed a postmortem assessment of the cerebral cortex of human neonates, and compared HX brains with appropriate controls. We found that expression of the activated (phosphorylated) EGFR was increased in the affected cortical areas in infants with HX. Therefore, we aimed to explore the functional role of EGFR-related signaling pathways in the cellular and molecular changes induced by HX in the cerebral cortex of newborn piglets. We established a regulatory role of EGFR kinase in the FAs network, by demonstrating that EGFR blockade before HX significantly reduced the cellular and anatomical damage induced by the injury. We also used RNA sequencing (RNA-seq) and transcriptomic bioinformatics to define for the first time gene regulatory networks induced by HX in the piglet cerebral cortex, and their regulation by EGFR signaling. Our transcriptomic analysis showed that a significant number of genes crucial for neuronal development and functional differentiation were differentially expressed during HX in piglet cortex, but were normalized following EGFR blockade. Importantly, a number of these genes are also known to be involved in human brain injury, further supporting the notion that phosphorylated EGFR plays a crucial role in HX-induced apoptotic cell death in the piglet and human perinatal brain (Dietrick et al., 2020; Korhonen et al., 1998; Maussion et al., 2019; Yu et al., 2016; Pardini et al., 2014; Yue et al., 2017).

RESULTS

HX Induces EGFR Activation in the Cerebral Cortex of Human Newborns

In a term neonate, acute HX mainly affects the cerebral cortex and basal ganglia. Therefore, we initially performed a neuropathological assessment of the cerebral cortex of postmortem human neonates with HX (n = 5) (Figure 1A, red box). We included neonates with the diagnosis of hypoxic-ischemic encephalopathy (moderate or severe) that were not subjected to hypothermia protocol for neuroprotection. We utilized postmortem brain tissue from subjects who succumb to sudden infant death syndrome to serve as controls (neonates without or with minimal exposure to HX and inflammation, n = 5) from National Institutes of Health NeuroBioBank (Table S1). Using H&E, we noticed that in neonates with HX the deep cortical layers (III–V) were depopulated, with numerous apoptotic profiles and profound edema, when compared with controls (Figure 1B). It has been demonstrated that HX activates the EGFR and its downstream cell death pathways (Chen et al., 2016; Delivoria-Papadopoulos et al., 2011a; Mishra et al., 2010; Scafidi et al., 2014). Therefore, we assessed expression of the activated EGFR in deep cortical layers and found enhanced expression of activated EGFR (number of phosphorylated EGFR-expressing cells) in the affected cortical areas of neonates with HX, when compared with controls (Figure 1C).

HX Induces EGFR Activation and Changes in Biochemical Energetics in Piglet Cortex

Based on our findings in the cortex of human neonates with HX, we assessed the effect of HX on EGFR function in the piglet cortex (Figure S1A). We first measured the enzymatic activity of EGFR. In line with our findings in human neonates, phosphorylated EGFR activity was significantly increased following HX (Figure S1B). To test the functional role of EGFR signaling in HX, we used a pharmacological inhibitor (EGFRi; PD-168393; 1 mg/kg) and established its potential to cross the blood-brain barrier by measuring enzymatic activity of the receptor in the brain. PD-168393 is a selective, cell-permeable pharmacologic compound with anti-tumor action that was initially used in cancer-related research for the treatment of EGFR-expressing tumors (Pu et al., 2006). Pretreatment with EGFRi significantly reduced the activity of EGFR kinase in the piglet cortex (Figure S1B), demonstrating its potential to cross the blood-brain barrier.

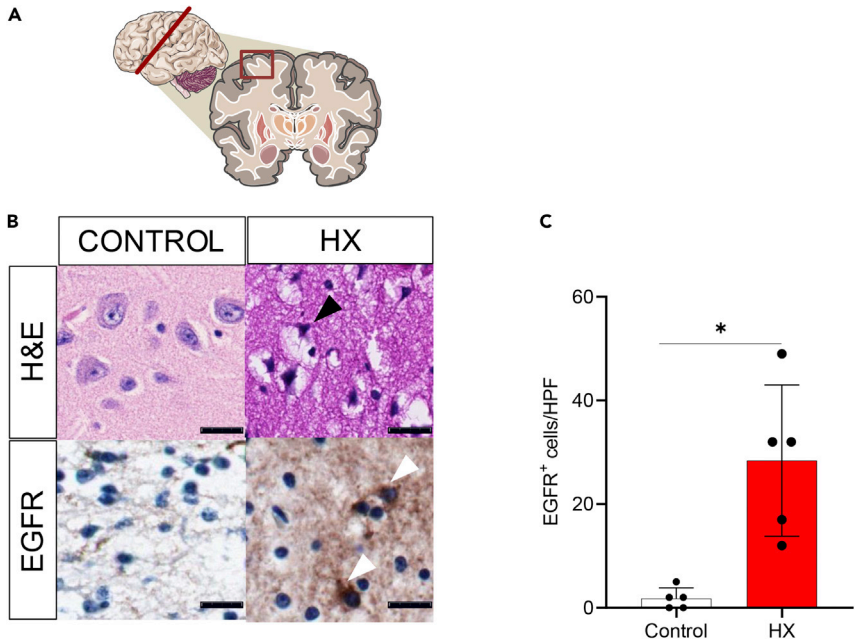

Figure 1. HX Induces EGFR Activation in the Cerebral Cortex of Human Newborns with HX

(A) Tissue sections from the parietal cerebral cortex of neonates with HX and controls were analyzed.

(B) Representative H&E photomicrographs. In controls, well-demarcated pyramidal neurons with well-defined nucleolus and dense neuropil were observed (upper left panel). In contrast, in HX (upper right panel) pyknotic neurons (black arrowhead) were present, with damaged irregular nucleolus, diffuse edematous matrix, and hypodense neuropil. Phosphorylated EGFR immunostaining (brown) is depicted in the lower panels. Almost no EGFR staining was present in the controls (lower left panel), whereas multiple cortical neurons were positive for EGFR in the HX group (white arrowheads).

(C) Immunostaining intensity from (B) is quantified as the number of EGFR-immunopositive cells. HX, hypoxic (n = 5), controls (n = 5). Data are represented as mean ± SD, t test *p < 0.05. (B) Photographed at 40X. Scale bar, 10 μm. This figure was created using Servier Medical Art templates, which are licensed under a Creative Commons Attribution 3.0 Unported License; https://smart.servier.com [smart.servier.com].

To optimize our study design, and ensure that all piglets exposed to HX (with and without EGFRi) achieved similar and comparable degree of injury, we performed direct biochemical measurements of two oxidative biometabolites—ATP and phosphocreatine (PCr)—in cortical tissue immediately after HX. The extent of HX in the piglet cortex was reflected in changes in biochemical energetics. Both ATP and PCr levels were significantly reduced in all HX groups, when compared with the normoxic (NX) groups (Figures S1C and S1D). No significant difference in cerebral tissue high-energy compounds was found in the HX groups with and without EGFRi, indicating that similar levels of HX were achieved in both groups (Figures S1C and S1D). Pretreatment with EGFRi did not reverse the energy failure due to HX. Finally, a number of physiological parameters examined were also similar in the HX and EGFRi-HX groups, and both groups displayed similar and significant differences from physiologic data obtained in NX piglets (Table S2), confirming that a similar degree of HX was achieved in HX and EGFRi-HX groups.

EGFR Blockade Attenuates the Neuropathological Alterations Induced by HX in Piglet Cerebral Cortex

Based on the biochemical results, we aimed to define the cellular effects of HX in the piglet cerebral cortex, and determined whether EGFRi pretreatment also affected HX-induced changes in cellular dynamics. First, we evaluated the overall cortical neuropathology following HX using H&E and a previously established and validated newborn piglet neuropathology score (Hoque et al., 2014; Kratimenos et al., 2017a, 2017b). The neuropathology score [median (interquartile range [IQR])] was 0 (0–1) in NX (n = 5) ($p < 0.05$ versus HX), 4 (3–4) in HX (n = 6) ($p < 0.05$ versus NX), and 2 (1–3) in EGFRi-HX (n = 7) ($p < 0.05$ versus HX) (Figures 2A–2C). In the superficial layers of the cortex (layers I and II), HX resulted in diffuse edema, very prominent laminar necrosis, disrupted neuropil, vacuolization, and a significant increase in necrotic neurons (Figures 2A, 2B, and 2D). Although we observed a positive trend, EGFRi did not significantly reverse the HX-induced edema

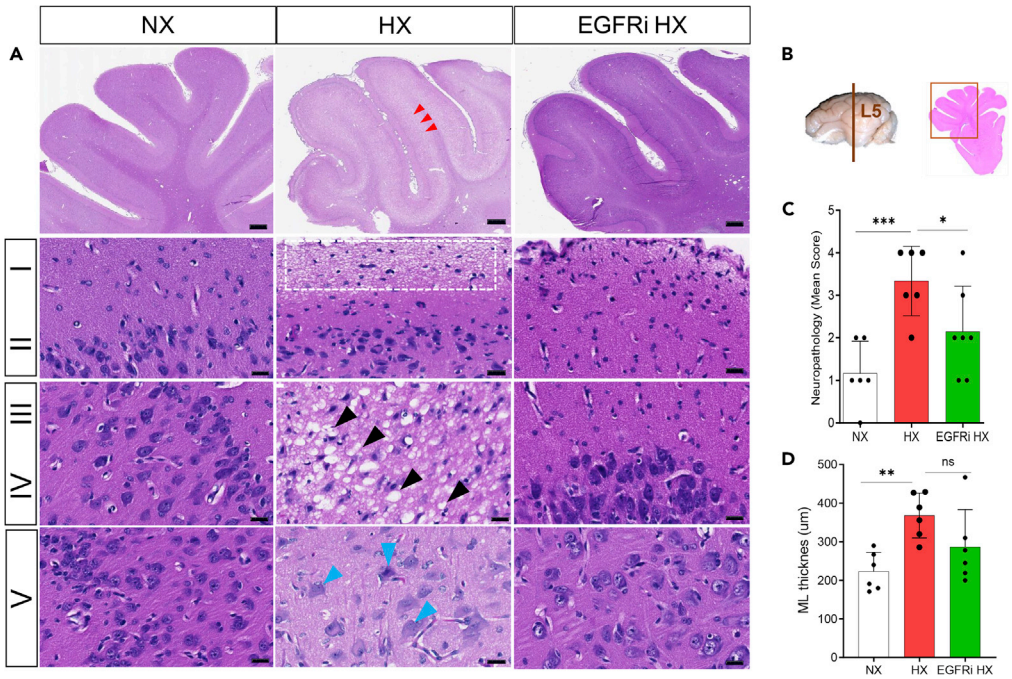

Figure 2. EGFR Blockade Attenuates Neuropathological Alterations Induced by HX in Piglet Cerebral Cortex

(A–D) (A–C) Representative photomicrographs of H&E staining from the cingulate and parietal cortex of NX, HX, and EGFRi HX piglets. In the superficial layers of the cerebral cortex (layers I–II), HX resulted in diffuse edema, very prominent laminar necrosis (depicted as pale zone, red arrowheads), disrupted neuropil (hatched box, layers I–II), vacuolization (black arrowheads, layers III–IV), and necrotic neurons (blue arrowheads, layer V). (A and D) The thickness of the molecular layer (ML) was increased in HX compared with NX. In the deep cortical layers (III–V), HX resulted in neuronal cell death hyperchromatic, pyknotic nuclei with ruptured and irregularly bordered nuclear membranes, and hypodense neuropil (A–C). In contrast, EGFRi blockade normalized or improved the neuropathological alterations observed in the HX group (C). The cortical neuropathology was assessed using a validated newborn piglet neuropathology score (Hoque et al., 2014) and the level of section was at level 5 (L5) based on the stereotaxic atlas of pig brain (Felix et al., 1999). NX, normoxic (n = 5), HX, hypoxic (n = 6); EGFRi HX, epidermal growth factor receptor blockade and HX (n = 7); ML, molecular layer; data are represented as mean ± SD, one-way ANOVA, *$p < 0.05$, **$p < 0.01$, ***$p < 0.001$. (A) Photographed at 2.5X (upper panel) and at 40X (lower panels). Scale bar, 100 μm in the upper and 20 μm in the lower panels (layers I –V). This figure was created using Servier Medical Art templates, which are licensed under a Creative Commons Attribution 3.0 Unported License; https://smart.servier.com [smart.servier.com].

of layers I and II in the cortex ($p = 0.06$, NS). In deep cortical layers III–V, HX resulted in neuronal cell death in the form of apoptosis, necrosis, or a continuum of hybrid forms, identified by hyperchromatic, pyknotic nuclei with ruptured and irregularly bordered nuclear membranes, and hypodense neuropil (Figure 2A). In contrast, EGFRi treatment resulted in fewer injured neurons, decreased number of apoptotic profiles, and the presence of well-defined round nuclei, i.e., it improved the overall neuropathology associated with HX (Figures 2A–2C).

EGFR Blockade Reverses HX-Induced Reduction in Neurons and Cell Death in Piglet Cerebral Cortex

Next, we determined the specific role of EGFR in neuronal survival in the piglet cortex. Positive immunostaining for NeuN was used as a mature neuronal marker. HX caused a decrease in the number of $NeuN^+$ neurons in deep cortical layers III–V (Figures 3A–3C), indicating that deep cortical neurons were significantly affected by injury. EGFRi blockade significantly reversed the effects of HX in neurons of these layers (Figures 3A–3C). In addition to neuropathology, DNA fragmentation was also assessed by terminal deoxynucleotidyl transferase-mediated nick end labeling (TUNEL) and immunofluorescence microscopy. NX piglets did not display any significant TUNEL labeling (Figures 3A, 3B, and 3D). HX increased the total number of TUNEL-labeled cells, but fewer TUNEL-positive cells were found in HX piglets treated with EGFRi (Figures 3A, 3B, and 3D). Finally, we evaluated overall cell survival by cleaved Caspase-3 immunostaining.

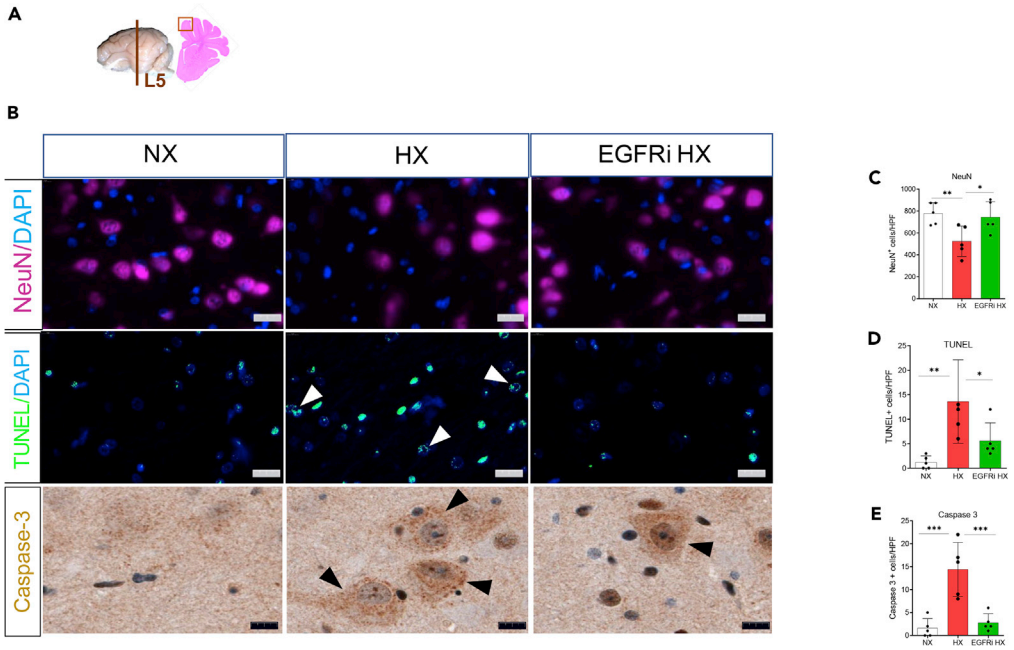

Figure 3. EGFR Blockade Reverses HX-Induced Reduction in Neurons and Cell Death in Piglet Cerebral Cortex

(A–E) (A and B) Representative photomicrographs of NeuN, TUNEL, and cleaved Caspase-3 immunostaining in layers III–V of the cingulate and parietal cortex (A) of NX, HX, and EGFRi HX piglets. HX resulted in a decrease in the number of NeuN+ neurons in the cortical layers III–V (B and C) and increased cell death, as shown by TUNEL+ and cleaved Caspase-3+ cells (B, D, and E). Pretreatment with EGFR blockade reversed the effects of HX on neurons as well as overall on cell death after injury (B–E). Note the characteristic apoptotic profiles in TUNEL+ cells (white arrowheads) and the cleaved Caspase-3+ cells (black arrowheads). TUNEL, terminal deoxynucleotidyl transferase dUTP nick end labeling; DAPI, 4′, 6-diamidino-2-phenylindole; NX, normoxic (n = 5), HX, hypoxic (n = 5); EGFRi HX, epidermal growth factor receptor blockade and HX (n = 5). Data are represented as mean ± SD, one-way ANOVA, *p < 0.05, **p < 0.01, ***p < 0.001. (B) Photographed at 60X (NeuN and TUNEL) and 100X (cleaved Caspase-3). Scale bar, 10 μm (NeuN and TUNEL) and 5 μm (cleaved Caspase-3).

HX caused a 4/5-fold increase in the number of cleaved Caspase-3+ cells (Figures 3A, 3B, and 3E), which was almost completely reversed by EGFRi treatment (Figures 3A, 3B, and 3E).

EGFR Blockade Reverses HX-Induced Gliosis in Piglet Cerebral Cortex

In the next set of experiments, we determined the specific role of the EGFR in the response of different types of glial cells to HX in the piglet cortex. HX induced a 3-fold increase in the number of GFAP+ reactive astrocytes and in Olig2+ GFAP+ cells (Figures 4A–4C), indicating that distinct glial cell types were affected by injury. Conversely, HX caused a significant decrease in the number of Olig2+ GFAP− oligodendrocyte lineage cells (Figures 4A and 4D), partially due to a reduction in cell proliferation, as demonstrated by anti-Ki67 immunostaining in GFAP− cells (Olig2+Ki67+ cells that do not express GFAP) (Figures 4A and 4E). Increased astrogliosis was due to enhanced cell proliferation, as demonstrated by anti-Ki67 immunostaining in GFAP+ astrocytes (Figures 4A and 4F). EGFRi treatment reversed the effects of HX on the number of Olig2+ oligodendrocytes, and normalized reactive gliosis after injury (Figures 4A–4C, 4E, and 4F). Finally, EGFRi treatment also reversed the overall inhibitory effects of HX on oligodendrocyte proliferation (Figures 4A and 4E). Altogether, these findings indicate that HX induces differential effects on distinct types of glia in the piglet cortex, i.e., causes reactive gliosis in astrocytes and inhibits oligodendrocyte lineage cell proliferation. Importantly, both effects are reversed by EGFR inhibition before HX, indicating that EGFR activation induces the reactive astrocytosis and the oligodendrocyte lineage injury following HX.

EGFR Blockade Reverses the Effects of HX on CaMKIV Activation in Piglet Cortex

We aimed to explore whether EGFR interferes with specific signaling pathways activated by HX in the piglet brain (Chakraborty et al., 2014; Chin et al., 1997; Ferriero, 2004; Jackson and Ceresa, 2017; Kratimenos et al.,

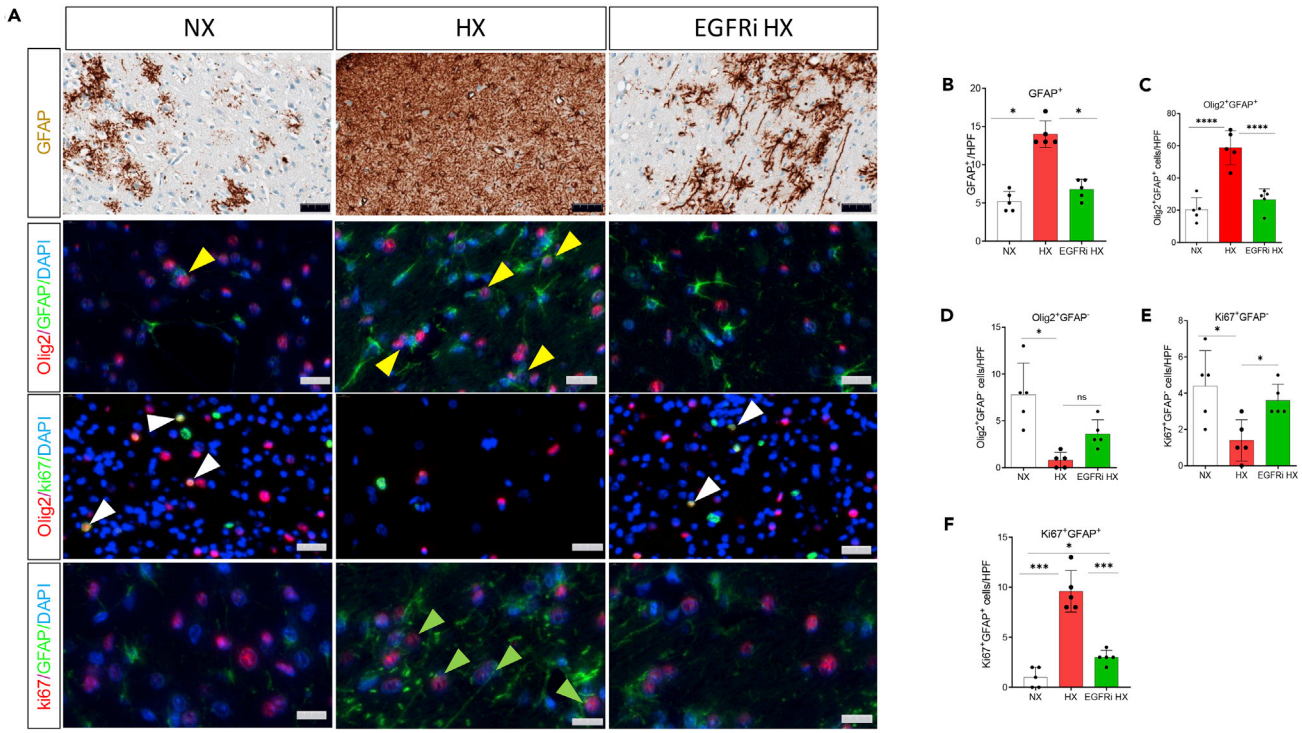

Figure 4. EGFR Blockade Reverses HX-Induced Gliosis in Piglet Cerebral Cortex

(A–F) (A) Representative photomicrographs of Olig2+, GFAP+, and Ki67+ cells from the cingulate and parietal cortex of NX, HX, and EGFRi HX piglets. (A, B, and C) HX induced a significant increase in the number of GFAP+ reactive astrocytes and of Olig2+ GFAP+ cells (yellow arrowheads). (A, D, and E) HX also caused a significant decrease in the number of Olig2+ GFAP− oligodendrocyte lineage cells, due to a reduction in cell proliferation, as demonstrated by the number of Olig2+Ki67+ that did not express GFAP (white arrowheads). (A and F) Anti-Ki67 immunostaining in GFAP+ cells (A, green arrowheads) indicates that increased astrogliosis was due to an increase in cell proliferation. (A, B, C, and F) EGFRi treatment reversed all the effects of HX on astrogliosis. (A and E) Finally, EGFRi treatment also reversed the overall inhibitory effects of HX on oligodendrocyte proliferation. GFAP, glial fibrillary acidic protein; Olig2, oligodendrocyte transcription factor; DAPI, 4′,6-diamidino-2-phenylindole; NX, normoxic (n = 5); HX, hypoxic (n = 5); EGFRi HX, epidermal growth factor receptor blockade and HX (n = 5). Data are represented as mean ± SD, one-way ANOVA, *p < 0.05, **p < 0.001, ****p < 0.0001; (A) Photographed at 40X (GFAP and Olig2/ki67) and at 60X (Olig2/GFAP and Ki67/GFAP). Scale bar, 10 μm in GFAP, Olig2/GFAP/DAPI, and Olig2/ki67/DAPI and 5 μm in ki67/GFAP/DAPI.

2017a; Soderling, 1999; Treda et al., 2016). As calcium plays a central role in cell signaling, we focused on the relationship between EGFR activation and intracellular Ca^{2+}. Expression of tyrosine-phosphorylated CaMKIV and its enzymatic activity were significantly enhanced in the piglet cortex after HX (Figures S2A and S2B). EGFRi treatment prevented HX-induced increase in CaMKIV expression and activity (Figures S2A and S2B), indicating that EGFR inhibition directly interfered with the calcium signaling pathway activated by HX in the piglet cortex.

Transcriptomic Changes Induced by HX in Piglet Cortex Are Reversed by EGFR Blockade

To further investigate molecular mechanisms underlying the effects of HX in the piglet cortex and to establish the functional role of EGFR, we defined the transcriptome of early postnatal piglet cerebral cortex using RNA-seq. All reported differentially expressed genes (DEGs) had normalized read counts above 5 in all samples and reached statistical significance (adjusted $p < 0.05$). Distinct expression patterns were evident between NX, HX, and EGFRi HX (Figure 5A). Differential gene expression analysis between the groups revealed 522 DEGs between HX and NX cerebral cortex tissue (318 up-regulated, 204 down-regulated), 786 DEGs between EGFRi-HX and HX (331 up-regulated, 456 down-regulated), and 158 DEGs between EGFRi-HX and NX (118 up-regulated and 40 down-regulated) (Figure 5A and Data S1, S2, and S3).

Interestingly, specific genes that are known to be involved in human brain injury, such as *BDNF, CAMKK2A, CAMK2A, DRD1, DRD2, FEZF2,* and *CREB5* (Dietrick et al., 2020; Korhonen et al., 1998; Maussion et al., 2019; Yu et al., 2016; Pardini et al., 2014; Yue et al., 2017), were also altered in the piglet cortex, further emphasizing the significance and clinical relevance of the piglet model of neonatal HX brain injury. The

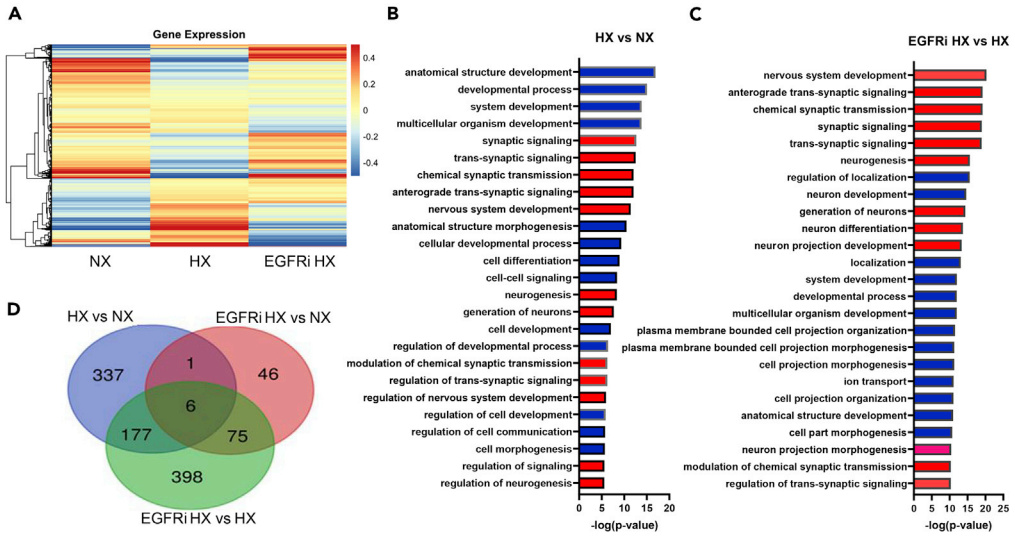

Figure 5. Transcriptomic Changes Induced by HX in Piglet Cortex Are Reversed by EGFR Blockade

(A) Heatmap of average expression of the total DEGs across the three study groups (NX, HX, and EGFRi HX). The color bar to the right indicates expression levels, where cool/blue represents lowest levels and warm/red indicates highest levels. Source data are provided as a Source Data file.

(B and C) Bar diagrams depicting the distribution of GO terms in HX versus NX and EGFRi HX versus HX. Criteria for inclusion as a highly enriched function required a –log adjusted p value of ≥ 5, shown by the horizontal p threshold line. DEGs based on statistical analysis using the Wald test with Benjamini-Hochberg correction (adjusted $p < 0.05$). GO terms in red color highlight nervous system-specific functions.

(D) Venn diagram depicting DEG overlap in HX versus NX, EGFRi HX versus HX, and EGFRi HX versus NX. GO, Gene Ontology; NX, normoxic (n = 2); HX, hypoxic (n = 3); EGFRi HX (n = 3), epidermal growth factor receptor blockade and HX. GO term lists, specific transcripts and names of genes associated with them are shown for (C) and (D) in Data S5 and S6.

above transcripts identified through RNA-seq as altered by HX and EGFRi HX were confirmed by RT-PCR (Figures S3A–S3G).

Next, using g:Profiler (Raudvere et al., 2019), we sorted DEGs via enriched functional Gene Ontology (GO) terms, to reveal HX-induced alterations in biological functions and to define the effects of EGFRi treatment (Figures 5B and 5C). Of the top 25 predicted biological functions to be altered in HX, 12 specifically represented functions of synaptic signaling, synaptic transmission, and regulation of nervous system development, neuronal differentiation, and neurogenesis. After EGFRi treatment, 13 of the top 25 biological functions were specifically associated with nervous system development (top enriched function), including neurogenesis, neuronal differentiation, and development of neuronal projections, and 6 GO terms were associated with synaptic signaling/synaptic transmission (HX versus NX: 521 DEG annotated genes, 142 human homologs; EGFRi-HX versus HX: 656 DEG annotated genes, 773 human homologs; EGFRi-HX versus NX: 128 DEG annotated genes, 37 human homologs) (Figures 5C and 5D and Data S4). A Venn diagram of overlap between the 3-group comparisons showed that HX resulted in 521 DEGs versus NX, and that 183 of these DEGs were also significantly altered by EGFRi (Figure 5D).

As neuronal development and synaptic transmission were predicted to be altered based on the GO analysis, heatmaps of DEGs from both groups were created. This analysis revealed distinct groups of DEGs related to these functions that were affected by HX, and were either responsive to EGFRi (Figures 6A and 6B) or unresponsive to EGFRi treatment (Figures 6C and 6D). Descriptive names for all genes are provided in Supplemental Data (Data S5 and S6). Of note, one of the neurotrophins, the brain-derived neurotrophic factor (BDNF), was significantly altered by HX and fully reversed by EGFRi treatment (Figures 6A, 6B, and S3G and Table S3).

HX Induces Transcriptional Alterations in Ca^{2+} and EGFR-Mediated Signaling Pathways that Are Prevented by EGFR Blockade

Next, we utilized Ingenuity Pathway Analysis (IPA; Qiagen) to identify specific canonical pathways and upstream regulators altered by HX either in the presence or absence of EGFR blockade. Importantly, EGFR

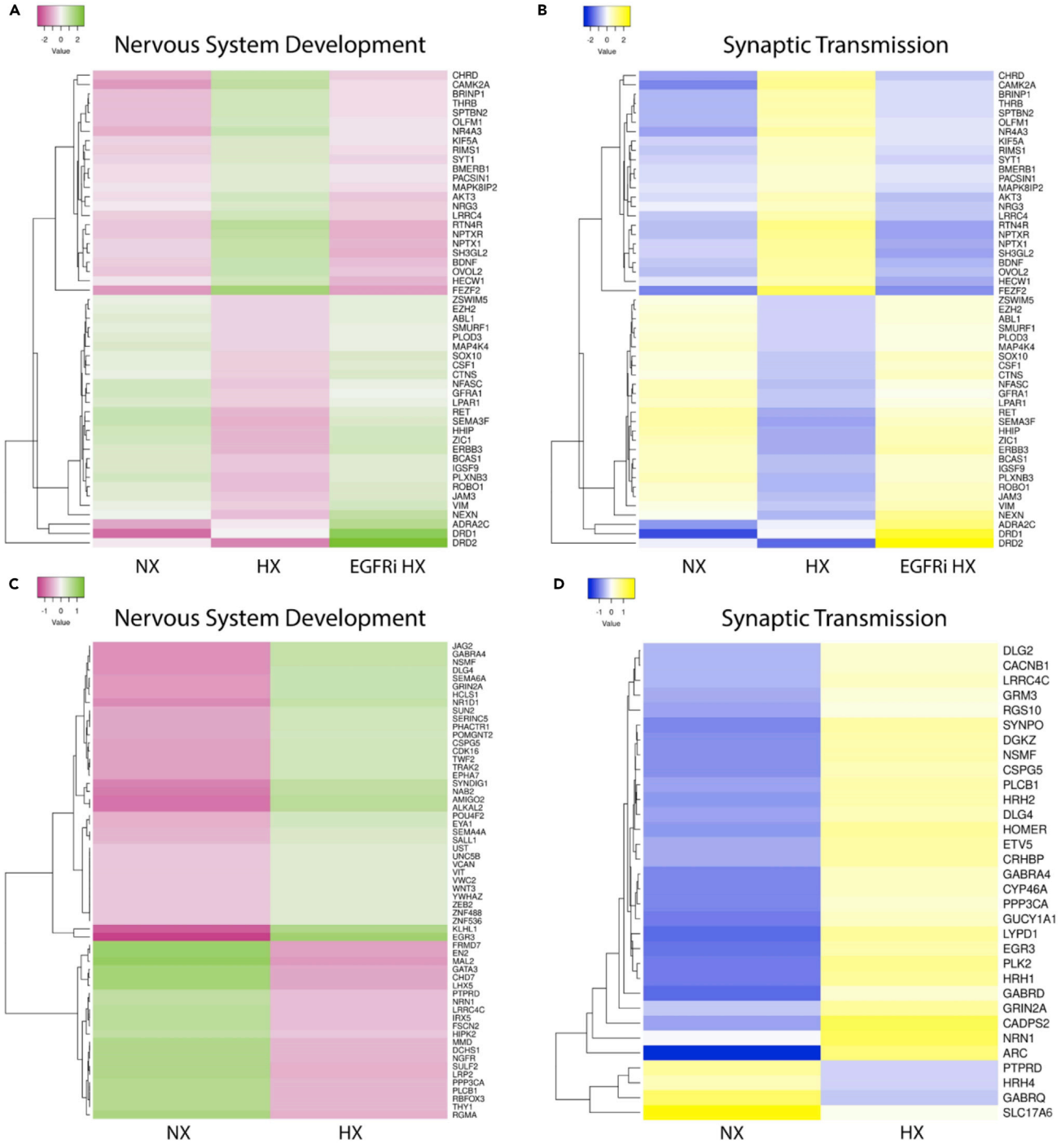

Figure 6. EGFR Blockade Normalizes HX-Induced Alterations in Specific DEGs Associated with Nervous System Development and Synaptic Transmission

(A–D) Heatmaps derived from genes identified in the GO term analysis that are associated with either nervous system development (A and C) or synaptic transmission (B and D). Expression levels of DEGs that were altered by HX and by HX EGFRi are shown in the top maps (A and B). On the bottom (C and D) DEGs that were altered by HX, but not by HX EGFRi are shown. Transcripts in (A) and (B) are distinct from those in (C) and (D), indicating that although EGFRi affects the expression of a broad group of genes altered by HX, other genes involved in neuronal development and synaptic transmission that are altered by HX are not affected by EGFRi. DEG, differentially expressed genes based on statistical analysis using the Wald test with Benjamini-Hochberg correction (adjusted $p < 0.05$). GO, Gene Ontology; NX, normoxic (n = 2); HX, hypoxic (n = 3); EGFRi HX (n = 3), epidermal growth factor receptor blockade and HX. Gene symbols and individual descriptions for the transcripts in the maps are shown in Data S5.

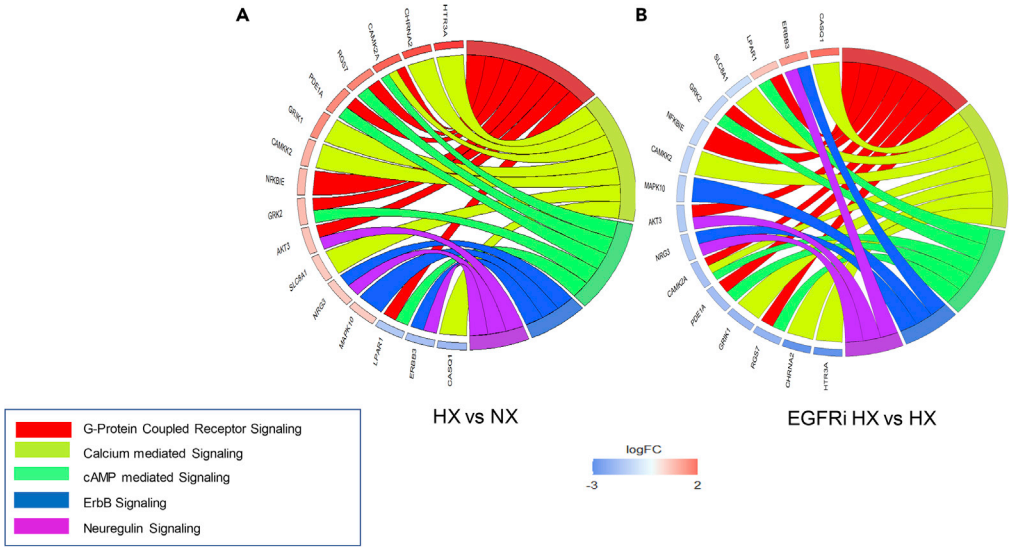

Figure 7. HX Induces Molecular Alterations in EGFR-Mediated Signaling Pathways That Are Prevented by EGFR Blockade

(A and B) Circos plots depicting the main EGFR-associated signaling pathways altered by HX (A) and reversed by EGFR blockade (B) in piglet cerebral cortex. Transcript symbols outside the circle depict individual DEGs. The log fold change (fc) for each DEG is shown in the outer circle bars where fc for HX versus NX is shown in (A) and fc for HX EGFRi versus HX is shown in (B). Interactions between EGFR-associated pathways are shown by the colored-coded connections; G-protein-coupled receptor signaling pathway (red), calcium-mediated signaling (light green), cAMP-mediated signaling (fluorescent green); ErbB signaling (blue), neuregulin signaling (purple). DEG, statistically differential expression of genes, using the Wald test with Benjamini-Hochberg correction (adjusted $p < 0.05$). NX, normoxic (n = 2); HX, hypoxic (n = 3); EGFRi HX (n = 3), epidermal growth factor receptor blockade and HX.

was identified as upstream regulator in HX-induced expression of many genes (*SCUBE3, NELL1, EDIL3, ERBB3, Neuregulin 3, GAB1, DRD1, DRD2, MAPK10, MAPK11, MAPK8IP2, MAP3K10, MAP3K5, MAP4K4, ABL, FEFZ2,* and *MAPK1*) (Figure 7A; see also Figures 5 and 6), and EGFR blockade normalized many of these alterations (Figure 7B). Interestingly, HX also altered the expression of numerous genes directly related to calcium signaling (Figure 7A). In line with our results on CaMKIV signaling, EGFR blockade reversed HX-induced transcriptomic alterations related to calcium signaling, indicating that EGFR mediates HX-induced neuronal injury through calcium signaling pathways (Figure 7B).

Of note, EGFR blockade also prevented HX-induced differential expression of genes related to G-protein, ErbB, cyclic AMP (cAMP), and Neuregulin signaling pathways (Figure 7B). G-proteins, cAMP, and ErbB signaling pathways play a significant role in cell proliferation and death, and their differential expression in the cerebral cortex might contribute to altered neuropathology and developmental disabilities. The Neuregulin pathway (*ERBB3, NRG3, AKT3*) plays a significant role in the plasticity of the developing brain and is known to have a protective role following HX injury (Corfas et al., 2004; Yoo et al., 2019).

Altogether, our RNA-seq analysis offers a wealth of new information regarding complex changes in specific gene networks that govern neuronal functions in the piglet brain under normal physiological conditions and after HX. This analysis also defines the impact of EGFR inhibition on a variety of dynamic molecular changes underlying cellular recovery from perinatal HX in the developing piglet cortex.

DISCUSSION

In the present study, we define a regulatory function of EGFR in acute HX of the cerebral cortex of the newborn piglet. We also establish a role of EGFR-associated signaling pathways in the molecular, cellular, and neuropathological outcome of the injury. Finally, we present for the first time a high-throughput analysis of the newborn piglet brain, which provides novel and crucial insights into HX-induced molecular alterations in neurotransmitters and neurotrophins, as well as abnormalities in neuronal development and synaptogenesis. Importantly, we identified genes that are directly associated with HX-induced EGFR

signaling that are also altered in human brain injury (Dietrick et al., 2020; Korhonen et al., 1998; Maussion et al., 2019; Yu et al., 2016; Pardini et al., 2014; Yue et al., 2017). Moreover, we identify transcripts regulated by HX that could not be mapped to the annotated pig genome, but were mapped to the more complete human genome (human homologs) (Data S4). Overall, these data not only support the significance of our molecular findings, but—more broadly—point to the translational impact of the piglet injury model used in this study.

EGFR kinase is a well-established promoter of cell proliferation, neuronal growth, and regeneration. However, EGFR activation may induce cell proliferation and growth in some cell populations, and apoptosis in others, depending on type of injury, brain region, and developmental stage of the brain (Armstrong et al., 1994; Jackson and Ceresa, 2017). Mice lacking EGFR die *in utero* or shortly after birth, or undergo significant neurodegeneration (Craig et al., 1996). Previous data in rodents revealed that EGFR promotes the progression of stem cells to proliferative progenitor cells (Kuhn et al., 1997), but plays different roles in distinct brain cell populations. In a mouse model of neonatal HX injury, activation of EGFR in glial progenitors promoted oligodendrocytes regeneration and timely developmental myelination, together with functional recovery (Scafidi et al., 2014). Conversely, administration of EGFR agonists negatively affected neurogenesis and neuroblast development (Koprivica et al., 2005; Kuhn et al., 1997). EGFR overexpression induced apoptosis in some neuronal cell lines through modification of the GluN2B subunit of the NMDA receptor (Tang et al., 2015). EGFR was also found to be highly expressed in brain malignancies; however, its overexpression was due to HX in the tumor core rather than to genetic alterations, which is consistent with the fact that human tumors that overexpress EGFR often lack a receptor mutation (Franovic et al., 2007).

Activation of the EGFR by auto-phosphorylation leads to binding of the adaptor protein Grb2 in the cytosol and activation of the Ras exchange factor Son of Sevenless (Sos). These molecular events result in activation of the Ras/MAPK signaling cascade, and downstream activation of nuclear mechanisms leading to Ca^{2+} influx in the nucleus itself, and CREB transcription and caspase-dependent cell death (Delivoria-Papadopoulos et al., 2008; Hognason et al., 2001). Our analysis in the developing piglet cerebral cortex shows that EGFR blockade before HX prevents injury-induced activation of nuclear enzymes. The activity of nuclear CaMKIV was enhanced by HX, but attenuated following EGFR inhibition, indicating that EGFR function also impacts nuclear function. In our previous studies, we demonstrated that inhibition of Src kinase following HX leads to attenuated neuropathological alterations and reduced activation of the nuclear enzymes (Kratimenos et al., 2017a, 2017b). Furthermore, decreased activation of CaMKIV is reflected in improved neuropathology in the neonatal brain (Kratimenos et al., 2017b). Based on these findings, it can be hypothesized that a functional cross talk between EGFR and Src kinases exists, ultimately resulting in downstream activation of nuclear CaMKIV.

The significant involvement of EGFR in HX-induced cortical injury and associated cellular outcomes highlights its importance as a potential target for therapeutic intervention. However, the precise molecular mechanisms that link HX to activation of EGFR and the ultimate cellular/neuropathological outcomes are still undefined. It has been shown that EGFR may interact with the SH2 homolog domain of the Src kinase leading to phosphorylation of the c-terminal of the molecule (Wagner et al., 2013). Conversely, Src can phosphorylate the EGFR kinase at a specific tyrosine residue (Y845), resulting in downstream activation of Ras/MAPK (Jackson and Ceresa, 2017). Therefore, targeting specific regulatory enzymes of the apoptotic pathway with small molecules may be an effective way to interrupt the neural cell death signaling cascade initiated by HX and EGFR activation.

Consistent with the notion of a crucial role of EGFR in HX-induced injury, we demonstrate that increased activation of EGFR kinase is reflected in significant neuropathological changes following HX of the newborn piglet brain, mainly in the deep layers of the cortex. We also show that EGFR blockade protects cortical neurons from HX-induced injury in deep cortical layers. It is hypothesized that the superficial layers of the cortex receive additional blood supply by the meningeal vessels, and thus become more resistant to HX. In agreement with our observations in human, the cortical layers III–V were more severely affected by HX, displaying highest levels of neuronal abnormalities, including cell death. Neurons of deep layers of the cerebral cortex highly express the Forebrain embryonic zinc finger 2 (*Fezf2*), which is important for the development of corticospinal projection neurons, as well as for differentiation of neuronal stem cells in the subventricular zone (Chen et al., 2005; Zuccotti et al., 2014). Our validated transcriptomic analysis

indicated that *Fezf2* was up-regulated in HX (by 2.5-fold, when compared with NX), whereas EGFR blockade totally prevented its up-regulation (Figure S3F). In the mature brain, *Fezf2* has a significant role in neuronal signaling and plasticity, and in cell adhesion molecules and calcium signaling pathways (Le Pichon et al., 2013). In summary, EGFR may play an important functional role in injury-induced alterations of *Fezf2* during a crucial developmental period, which may ultimately result in disrupted deep cortical neuronal signaling and plasticity of the developing brain.

In addition to extensive effects of EGFR-mediated HX injury on neurons, our analysis also revealed a role for EGFR signaling in HX-induced glial cell activation in the piglet cerebral cortex after HX. However, HX had distinct effects on astrocytes and oligodendrocytes, as it promoted astrocyte proliferation, but reduced oligodendrocyte lineage cell proliferation and number. These findings are consistent with analysis in human brain showing that neonatal HX causes reactive gliosis, as well as reduced oligodendrocyte maturation and myelination (Dean et al., 2011; Bruce and Becker, 1991; Back, 2017). The opposite effects of HX on astrocytes and oligodendrocytes were reversed by EGFR blockade, demonstrating that the EGFR pathway plays different roles in distinct glial cell types. Future analysis will further investigate the intracellular signaling pathways associated with EGFR in these glial cell types, to define the molecular mechanisms leading to opposite cellular outcomes.

To elucidate the molecular underpinnings of the cellular effects induced by HX, and to gain further mechanistic insight into the functional role of EGFR, we performed high-throughput analysis of the piglet cerebral cortex under different experimental conditions. Our analysis revealed that HX-induced alterations related to calcium signaling, synaptogenesis, and neuronal cell proliferation and death were normalized by EGFR blockade. Furthermore, our molecular analysis revealed that genes involved in cell death pathways, including calcium, cAMP, erbB, Neuregulin, and G-protein signaling, were significantly altered during HX, and EGFR blockade prevented their differential expression. In particular, HX-induced EGFR phosphorylation mediated activation of the apoptotic pathway through a variety of regulatory molecules of calcium signaling, including *CAMK2A, CAMKIV, CAMKK2,* and *CREB5*. EGFR blockade completely reversed the differential expression of these genes, resulting in normalization of CAMKIV, Caspase-3, and TUNEL, and ultimately attenuated neuropathological alterations.

Importantly, BDNF was significantly altered by HX and fully reversed by EGFRi treatment. BDNF has been shown to be a main biomarker in human neonatal HX encephalopathy, with most studies suggesting lower levels of BDNF during HX (Dietrick et al., 2020; Korhonen et al., 1998; Liu et al., 2013). BDNF promotes the survival and differentiation of neurons, mediates axonal growth and pathfinding, and promotes dendritic growth and morphological maturation. BDNF also contributes to adaptive neuronal responses and synaptic plasticity, as well as homeostatic regulation of intrinsic neuronal excitability (Failla et al., 2016; Munoz et al., 2017).

Interestingly, other genes related with EGFR signaling were differentially expressed in HX. Among these, we identified a subset of genes that are known to be important for brain development, such as the dopamine D_1 and D_2 (*DRD1* and *DRD2*) receptors. Dopamine receptors are known to be involved in brain development, neuronal cell migration, and formation of connectivity, as well as in neuropsychiatric diseases such as schizophrenia, or drug addiction and motor learning disabilities (Sillivan and Konradi, 2011; Bertran-Gonzalez et al., 2008). These results suggest that some of the long-term functional abnormalities observed after HX in the human brain might be, at least in part, mediated by alterations in dopamine receptor signaling.

In conclusion, our analysis of the developing piglet cerebral cortex defines many new exciting avenues of scientific exploration to further elucidate the beneficial impact of EGFR blockade on perinatal brain injury at the cellular and molecular levels. This analysis could potentially result in the identification of new therapeutic targets associated with EGFR signaling in the developing mammalian brain that are linked with specific long-term abnormalities caused by perinatal brain injury.

Limitation of the Study

We acknowledge several limitations to our study. Our main goal in this study was to understand mechanistically how EGFR phosphorylation (activation) during HX results in neuronal injury and whether inhibition of EGFR can prevent neuronal injury during HX. Therefore, we chose to administer the inhibitor 30 min before HX. Using a stepwise approach, now that we have demonstrated that HX-induced activation of EGFR is a mechanism involved in neuronal damage, our next goal is to study the effect of EGFR inhibition following

HX at different time points after HX. We will address time points after induction of HX. We will also test EGFR inhibition in combination with therapeutic hypothermia for HX ischemia.

Resource Availability

Lead Contact

Further information and requests for resources and reagents should be directed to and will be fulfilled by the Lead Contact, Dr. Vittorio Gallo (vgallo@childrensnational.org).

Material Availability

This study did not generate new unique reagents.

Data and Code Availability

The RNA sequencing data have been deposited to Sequence Read Archive (SRA) database (Submission ID: SUB8338144, BioProject ID: PRJNA670468, accession link: https://submit.ncbi.nlm.nih.gov/subs/sra/SUB8338144/overview). Histology and western blot and PCR data are available upon request by Dr. Gallo and Dr. Kratimenos. Enzyme activity data and biological experiment information are available at Dr. Delivoria-Papadopoulos' lab at Drexel University.

METHODS

All methods can be found in the accompanying Transparent Methods supplemental file.

SUPPLEMENTAL INFORMATION

Supplemental Information can be found online at https://doi.org/10.1016/j.isci.2020.101766.

ACKNOWLEDGMENTS

This work was supported by NICHD-20337 (PI: M.D.-P.), R37NS109478 (PI: V.G.), and the District of Columbia Intellectual and Developmental Disabilities Research Center (DC-IDDRC) U54HD090257 (PI: V.G.) and the Clinical and Translational Science Award (CTSA) UL1TR001876 (PI: Lisa Guay-Woodford, MD). We acknowledge the support of a Children's National Board of Visitors Grant (PI: P.K.) and a K12-HD-001339 (NICHD) (PI: I.K.). We also acknowledge the support of the Children's National Research Institute Bioinformatics Unit. Its contents are solely the responsibility of the authors and do not necessarily represent the official views of the National Institutes of Health. We thank the Johns Hopkins University Genome Sciences and Bioinformatics core for NovaSEQ access. We thank Dr. Karuna Panchapakesan (Genomics Core) for the technical support.

We would like to dedicate this work in memory of our beloved mentor, colleague, and friend, M.D.-P., for her dedication to science, mentorship, kindness, and devotion to young scientists, who sadly passed away on September 11, 2020, during the initial revision of this paper.

AUTHORS CONTRIBUTION

M.D.-P., P.K., and V.G. conceived and designed the experiments. P.K., E.Z.G., S.M., B.J., S.K., and K.P. performed the experiments. P.K. and I.A.-S. obtained and analyzed the human data. P.K. wrote the main manuscript text. M.D.-P. and V.G. supervised the experiments and edited the manuscript. P.K., I.K., and I.A.-S. reviewed the H&E, immunostainings, and TUNEL slides and scored the neuropathology. P.K. and P.B. did the statistics. P.K. and I.K. prepared the figures and wrote the statistic section of the manuscript. S.K. and K.P. performed the RNA sequencing library and E.Z.G. analyzed the transcriptomic data. P.B. performed the bioinformatics analysis. All authors reviewed and revised the manuscript.

DECLARATION OF INTERESTS

The authors declare no competing interests.

Received: September 1, 2020
Revised: October 12, 2020
Accepted: October 30, 2020
Published: December 18, 2020

REFERENCES

Armstrong, D.K., Kaufmann, S.H., Ottaviano, Y.L., Furuya, Y., Buckley, J.A., Isaacs, J.T., and Davidson, N.E. (1994). Epidermal growth factor-mediated apoptosis of MDA-MB-468 human breast cancer cells. Cancer Res. *54*, 5280–5283.

Back, S.A. (2017). White matter injury in the preterm infant: pathology and mechanisms. Acta Neuropathol. *134*, 331–349.

Bertran-Gonzalez, J., Bosch, C., Maroteaux, M., Matamales, M., Herve, D., Valjent, E., and Girault, J.A. (2008). Opposing patterns of signaling activation in dopamine D1 and D2 receptor-expressing striatal neurons in response to cocaine and haloperidol. J. Neurosci. *28*, 5671–5685.

Bjorkman, S.T., Foster, K.A., O'driscoll S, M., Healy, G.N., Lingwood, B.E., Burke, C., and Colditz, P.B. (2006). Hypoxic/Ischemic models in newborn piglet: comparison of constant FiO2 versus variable FiO2 delivery. Brain Res. *1100*, 110–117.

Brambrink, A.M., Martin, L.J., Hanley, D.F., Becker, K.J., Koehler, R.C., and Traystman, R.J. (1999). Effects of the AMPA receptor antagonist NBQX on outcome of newborn pigs after asphyxic cardiac arrest. J. Cereb. Blood Flow Metab. *19*, 927–938.

Bruce, K., and Becker, L.E. (1991). Quantitation of medullary astrogliosis in sudden infant death syndrome. Pediatr. Neurosurg. *17*, 74–79.

Chakraborty, S., Li, L., Puliyappadamba, V.T., Guo, G., Hatanpaa, K.J., Mickey, B., Souza, R.F., Vo, P., Herz, J., Chen, M.R., et al. (2014). Constitutive and ligand-induced EGFR signalling triggers distinct and mutually exclusive downstream signalling networks. Nat. Commun. *5*, 5811.

Chen, B., Schaevitz, L.R., and Mcconnell, S.K. (2005). Fezl regulates the differentiation and axon targeting of layer 5 subcortical projection neurons in cerebral cortex. Proc. Natl. Acad. Sci. U S A *102*, 17184–17189.

Chen, Z.D., Xu, L., Tang, K.K., Gong, F.X., Liu, J.Q., Ni, Y., Jiang, L.Z., Hong, J., Han, F., Li, Q., et al. (2016). NF-kappaB-dependent transcriptional upregulation of cyclin D1 exerts cytoprotection against hypoxic injury upon EGFR activation. Exp. Cell Res. *347*, 52–59.

Chin, Y.E., Kitagawa, M., Kuida, K., Flavell, R.A., and Fu, X.Y. (1997). Activation of the STAT signaling pathway can cause expression of caspase 1 and apoptosis. Mol. Cell Biol. *17*, 5328–5337.

Corfas, G., Roy, K., and Buxbaum, J.D. (2004). Neuregulin 1-erbB signaling and the molecular/cellular basis of schizophrenia. Nat. Neurosci. *7*, 575–580.

Craig, C.G., Tropepe, V., Morshead, C.M., Reynolds, B.A., Weiss, S., and Van Der Kooy, D. (1996). In vivo growth factor expansion of endogenous subependymal neural precursor cell populations in the adult mouse brain. J. Neurosci. *16*, 2649–2658.

Dean, J.M., Moravec, M.D., Grafe, M., Abend, N., Ren, J., Gong, X., Volpe, J.J., Jensen, F.E., Hohimer, A.R., and Back, S.A. (2011). Strain-specific differences in perinatal rodent oligodendrocyte lineage progression and its correlation with human. Dev. Neurosci. *33*, 251–260.

Delivoria-Papadopoulos, M., Ashraf, Q.M., Ara, J., and Mishra, O.P. (2008). Nuclear mechanisms of hypoxic cerebral injury in the newborn: the role of caspases. Semin. Perinatol. *32*, 334–343.

Delivoria-Papadopoulos, M., Ashraf, Q.M., and Mishra, O.P. (2011a). Brain tissue energy dependence of CaM kinase IV cascade activation during hypoxia in the cerebral cortex of newborn piglets. Neurosci. Lett. *491*, 113–117.

Delivoria-Papadopoulou, M., and Malaeb, S. (2014). Effect of concurrent administration of apoptotic inhibitors and hypothermia on post hypoxic cerebral injury in the newborn. Hell J. Nucl. Med. *17* (*Suppl 1*), 24–25.

Dietrick, B., Molloy, E., Massaro, A.N., Strickland, T., Zhu, J., Slevin, M., Donoghue, V., Sweetman, D., Kelly, L., O'dea, M., et al. (2020). Plasma and CSF candidate biomarkers of neonatal encephalopathy severity and neurodevelopmental outcomes. J. Pediatr. https://doi.org/10.1016/j.jpeds.2020.06.078.

Digiacomo, J.E., Pane, C.R., Gwiazdowski, S., Mishra, O.P., and Delivoria-Papadopoulos, M. (1992). Effect of graded hypoxia on brain cell membrane injury in newborn piglets. Biol. Neonate *61*, 25–32.

Ezzati, M., Kawano, G., Rocha-Ferreira, E., Alonso-Alconada, D., Hassell, J.K., Broad, K.D., Fierens, I., Fleiss, B., Bainbridge, A., Price, D.L., et al. (2017). Dexmedetomidine combined with therapeutic hypothermia is associated with cardiovascular instability and neurotoxicity in a piglet model of perinatal asphyxia. Dev. Neurosci. *39*, 156–170.

Failla, M.D., Conley, Y.P., and Wagner, A.K. (2016). Brain-derived neurotrophic factor (BDNF) in traumatic brain injury-related mortality: interrelationships between genetics and acute systemic and central nervous system BDNF profiles. Neurorehabil. Neural. Repair *30*, 83–93.

Felix, B., Leger, M.E., Albe-Fessard, D., Marcilloux, J.C., Rampin, O., and Laplace, J.P. (1999). Stereotaxic atlas of the pig brain. Brain Res. Bull. *49*, 1–137.

Ferriero, D.M. (2004). Neonatal brain injury. N. Engl. J. Med. *351*, 1985–1995.

Forster, R., Ancian, P., Fredholm, M., Simianer, H., Whitelaw, B., and Steering Group of the, R.P. (2010). The minipig as a platform for new technologies in toxicology. J. Pharmacol. Toxicol. Methods *62*, 227–235.

Franovic, A., Gunaratnam, L., Smith, K., Robert, I., Patten, D., and Lee, S. (2007). Translational up-regulation of the EGFR by tumor hypoxia provides a nonmutational explanation for its overexpression in human cancer. Proc. Natl. Acad. Sci. U S A *104*, 13092–13097.

Groenendaal, F., De Graaf, R.A., Van Vliet, G., and Nicolay, K. (1999). Effects of hypoxia-ischemia and inhibition of nitric oxide synthase on cerebral energy metabolism in newborn piglets. Pediatr. Res. *45*, 827–833.

Guerguerian, A.M., Brambrink, A.M., Traystman, R.J., Huganir, R.L., and Martin, L.J. (2002). Altered expression and phosphorylation of N-methyl-D-aspartate receptors in piglet striatum after hypoxia-ischemia. Brain Res. Mol. Brain Res. *104*, 66–80.

Haaland, K., Loberg, E.M., Steen, P.A., and Thoresen, M. (1997). Posthypoxic hypothermia in newborn piglets. Pediatr. Res. *41*, 505–512.

Hognason, T., Chatterjee, S., Vartanian, T., Ratan, R.R., Ernewein, K.M., and Habib, A.A. (2001). Epidermal growth factor receptor induced apoptosis: potentiation by inhibition of Ras signaling. FEBS Lett. *491*, 9–15.

Hoque, N., Sabir, H., Maes, E., Bishop, S., and Thoresen, M. (2014). Validation of a neuropathology score using quantitative methods to evaluate brain injury in a pig model of hypoxia ischaemia. J. Neurosci. Methods *230*, 30–36.

Imai, H., Konno, K., Nakamura, M., Shimizu, T., Kubota, C., Seki, K., Honda, F., Tomizawa, S., Tanaka, Y., Hata, H., and Saito, N. (2006). A new model of focal cerebral ischemia in the miniature pig. J. Neurosurg. *104*, 123–132.

Ishibashi, N., Scafidi, J., Murata, A., Korotcova, L., Zurakowski, D., Gallo, V., and Jonas, R.A. (2012). White matter protection in congenital heart surgery. Circulation *125*, 859–871.

Jackson, N.M., and Ceresa, B.P. (2017). EGFR-mediated apoptosis via STAT3. Exp. Cell Res. *356*, 93–103.

Jain, A., Kratimenos, P., Koutroulis, I., Jain, A., Buddhavarapu, A., and Ara, J. (2017). Effect of intranasally delivered rh-VEGF165 on angiogenesis following cerebral hypoxia-ischemia in the cerebral cortex of newborn piglets. Int. J. Mol. Sci. *18*, 2356.

Koprivica, V., Cho, K.S., Park, J.B., Yiu, G., Atwal, J., Gore, B., Kim, J.A., Lin, E., Tessier-Lavigne, M., Chen, D.F., and He, Z. (2005). EGFR activation mediates inhibition of axon regeneration by myelin and chondroitin sulfate proteoglycans. Science *310*, 106–110.

Korhonen, L., Riikonen, R., Nawa, H., and Lindholm, D. (1998). Brain derived neurotrophic factor is increased in cerebrospinal fluid of children suffering from asphyxia. Neurosci. Lett. *240*, 151–154.

Kratimenos, P., Koutroulis, I., Marconi, D., Syriopoulou, V., Delivoria-Papadopoulos, M., Chrousos, G.P., and Theocharis, S. (2014). Multi-targeted molecular therapeutic approach in aggressive neuroblastoma: the effect of Focal Adhesion Kinase-Src-Paxillin system. Expert Opin. Ther. Targets *18*, 1395–1406.

Kratimenos, P., Koutroulis, I., Agarwal, B., Theocharis, S., and Delivoria-Papadopoulos, M. (2017a). Effect of Src kinase inhibition on cytochrome c, smac/DIABLO and apoptosis inducing factor (AIF) following cerebral hypoxia-ischemia in newborn piglets. Sci. Rep. *7*, 16664.

Kratimenos, P., Koutroulis, I., Jain, A., Malaeb, S., and Delivoria-Papadopoulos, M. (2017b). Effect of concurrent Src kinase inhibition with short-duration hypothermia on Ca2+/calmodulin kinase IV activity and neuropathology after hypoxia-ischemia in the newborn swine brain. Neonatology *113*, 37–43.

Kratimenos, P., Koutroulis, I., Syriopoulou, V., Michailidi, C., Delivoria-Papadopoulos, M., Klijanienko, J., and Theocharis, S. (2017c). FAK-Src-paxillin system expression and disease outcome in human neuroblastoma. Pediatr. Hematol. Oncol. *34*, 221–230.

Kuhn, H.G., Winkler, J., Kempermann, G., Thal, L.J., and Gage, F.H. (1997). Epidermal growth factor and fibroblast growth factor-2 have different effects on neural progenitors in the adult rat brain. J. Neurosci. *17*, 5820–5829.

Kurinczuk, J.J., White-Koning, M., and Badawi, N. (2010). Epidemiology of neonatal encephalopathy and hypoxic-ischaemic encephalopathy. Early Hum. Dev. *86*, 329–338.

Lawn, J.E., Cousens, S., and Zupan, J.; Lancet Neonatal Survival Steering Team (2005). 4 million neonatal deaths: when? Where? Why? Lancet *365*, 891–900.

Liu, F., Yang, S., Du, Z., and Guo, Z. (2013). Dynamic changes of cerebral-specific proteins in full-term newborns with hypoxic–ischemic encephalopathy. Cell Biochem. Biophys. *66*, 389–396.

Martin, L.J., Brambrink, A., Koehler, R.C., and Traystman, R.J. (1997a). Primary sensory and forebrain motor systems in the newborn brain are preferentially damaged by hypoxia-ischemia. J. Comp. Neurol. *377*, 262–285.

Martin, L.J., Brambrink, A.M., Lehmann, C., Portera-Cailliau, C., Koehler, R., Rothstein, J., and Traystman, R.J. (1997b). Hypoxia-ischemia causes abnormalities in glutamate transporters and death of astroglia and neurons in newborn striatum. Ann. Neurol. *42*, 335–348.

Maulik, D., Ashraf, Q.M., Mishra, O.P., and Delivoria-Papadopoulos, M. (2008). Effect of hypoxia on protein tyrosine phosphatase activity and expression of protein tyrosine phosphatases PTP-1B, PTP-SH1 and PTP-SH2 in the cerebral cortex of Guinea pig fetus. Neurosci. Lett. *432*, 174–178.

Maussion, G., Moalic, J.M., Simonneau, M., Gorwood, P., and Ramoz, N. (2019). Increased expression of BDNF mRNA in the frontal cortex of autistic patients. Behav. Brain Res. *359*, 903–909.

Mehmet, H., Yue, X., Squier, M.V., Lorek, A., Cady, E., Penrice, J., Sarraf, C., Wylezinska, M., Kirkbride, V., Cooper, C., et al. (1994). Increased apoptosis in the cingulate sulcus of newborn piglets following transient hypoxia-ischaemia is related to the degree of high energy phosphate depletion during the insult. Neurosci. Lett. *181*, 121–125.

Mehmet, H., Yue, X., Penrice, J., Cady, E., Wyatt, J.C., Sarraf, C., Squier, M., and Edwards, A.D. (1998). Relation of impaired energy metabolism to apoptosis and necrosis following transient cerebral hypoxia-ischaemia. Cell Death Differ. *5*, 321–329.

Mishra, O.P., Ashraf, Q.M., and Delivoria-Papadopoulos, M. (2009). NO-mediated activation of Src kinase during hypoxia in the cerebral cortex of newborn piglets. Neurosci. Lett. *460*, 61–65.

Mishra, O.P., Ashraf, Q.M., and Delivoria-Papadopoulos, M. (2010). Hypoxia-induced activation of epidermal growth factor receptor (EGFR) kinase in the cerebral cortex of newborn piglets: the role of nitric oxide. Neurochem. Res. *35*, 1471–1477.

Munoz, M.J., Kumar, R.G., Oh, B.M., Conley, Y.P., Wang, Z., Failla, M.D., and Wagner, A.K. (2017). Cerebrospinal fluid cortisol mediates brain-derived neurotrophic factor relationships to mortality after severe TBI: a prospective cohort study. Front. Mol. Neurosci. *10*, 44.

Odden, J.P., Stiris, T., Hansen, T.W., and Bratlid, D. (1989). Cerebral blood flow during experimental hypoxaemia and ischaemia in the newborn piglet. Acta Paediatr. Scand. Suppl. *360*, 13–19.

Pardini, M., Krueger, F., Hodgkinson, C.A., Raymont, V., Strenziok, M., Amore, M., Wassermann, E.M., Goldman, D., and Grafman, J.H. (2014). Aggression, DRD1 polymorphism, and lesion location in penetrating traumatic brain injury. CNS Spectr. *19*, 382–390.

Le Pichon, C.E., Dominguez, S.L., Solanoy, H., Ngu, H., Lewin-Koh, N., Chen, M., Eastham-Anderson, J., Watts, R., and Scearce-Levie, K. (2013). EGFR inhibitor erlotinib delays disease progression but does not extend survival in the SOD1 mouse model of ALS. PLoS One *8*, e62342.

Pu, Y.S., Hsieh, M.W., Wang, C.W., Liu, G.Y., Huang, C.Y., Lin, C.C., Guan, J.Y., Lin, S.R., and Hour, T.C. (2006). Epidermal growth factor receptor inhibitor (PD168393) potentiates cytotoxic effects of paclitaxel against androgen-independent prostate cancer cells. Biochem. Pharmacol. *71*, 751–760.

Raudvere, U., Kolberg, L., Kuzmin, I., Arak, T., Adler, P., Peterson, H., and Vilo, J. (2019). g:Profiler: a web server for functional enrichment analysis and conversions of gene lists (2019 update). Nucleic Acids Res. *47*, W191–W198.

Scafidi, J., Hammond, T.R., Scafidi, S., Ritter, J., Jablonska, B., Roncal, M., Szigeti-Buck, K., Coman, D., Huang, Y., Mccarter, R.J., Jr., et al. (2014). Intranasal epidermal growth factor treatment rescues neonatal brain injury. Nature *506*, 230–234.

Sillivan, S.E., and Konradi, C. (2011). Expression and function of dopamine receptors in the developing medial frontal cortex and striatum of the rat. Neuroscience *199*, 501–514.

Soderling, T.R. (1999). The Ca-calmodulin-dependent protein kinase cascade. Trends Biochem. Sci. *24*, 232–236.

Tang, Y., Ye, M., Du, Y., Qiu, X., Lv, X., Yang, W., and Luo, J. (2015). EGFR signaling upregulates surface expression of the GluN2B-containing NMDA receptor and contributes to long-term potentiation in the hippocampus. Neuroscience *304*, 109–121.

Thoresen, M., Haaland, K., Loberg, E.M., Whitelaw, A., Apricena, F., Hanko, E., and Steen, P.A. (1996). A piglet survival model of posthypoxic encephalopathy. Pediatr. Res. *40*, 738–748.

Treda, C., Popeda, M., Ksiazkiewicz, M., Grzela, D.P., Walczak, M.P., Banaszczyk, M., Peciak, J., Stoczynska-Fidelus, E., and Rieske, P. (2016). EGFR activation leads to cell death independent of PI3K/AKT/mTOR in an AD293 cell line. PLoS One *11*, e0155230.

Vibert, Y.M., Ashraf, Q.M., Mishra, O.P., and Delivoria-Papadopoulos, M. (2008). Mechanism of Ca2+-influx and Ca2+/calmodulin-dependent protein kinase IV activity during in utero hypoxia in cerebral cortical neuronal nuclei of the Guinea pig fetus at term. Neurosci. Lett. *440*, 227–231.

Wagner, M.J., Stacey, M.M., Liu, B.A., and Pawson, T. (2013). Molecular mechanisms of SH2- and PTB-domain-containing proteins in receptor tyrosine kinase signaling. Cold Spring Harb. Perspect. Biol. *5*, a008987.

Yoo, S.Y., Yoo, J.Y., Kim, H.B., Baik, T.K., Lee, J.H., and Woo, R.S. (2019). Neuregulin-1 protects neuronal cells against damage due to CoCl2-induced hypoxia by suppressing hypoxia-inducible factor-1alpha and P53 in SH-SY5Y cells. Int. Neurourol J. *23*, S111–S118.

Yu, P., Chen, X., Zhao, W., Zhang, Z., Zhang, Q., Han, B., Zhai, J., Chen, M., Du, B., Deng, X., et al. (2016). Effect of rs1063843 in the CAMKK2 gene on the dorsolateral prefrontal cortex. Hum. Brain Mapp. *37*, 2398–2406.

Yue, X., Mehmet, H., Penrice, J., Cooper, C., Cady, E., Wyatt, J.S., Reynolds, E.O., Edwards, A.D., and Squier, M.V. (1997). Apoptosis and necrosis in the newborn piglet brain following transient cerebral hypoxia-ischaemia. Neuropathol. Appl. Neurobiol. *23*, 16–25.

Yue, J.K., Winkler, E.A., Rick, J.W., Burke, J.F., Mcallister, T.W., Oh, S.S., Burchard, E.G., Hu, D., Rosand, J., Temkin, N.R., et al. (2017). DRD2 C957T polymorphism is associated with improved 6-month verbal learning following traumatic brain injury. Neurogenetics *18*, 29–38.

Zuccotti, A., Le Magueresse, C., Chen, M., Neitz, A., and Monyer, H. (2014). The transcription factor Fezf2 directs the differentiation of neural stem cells in the subventricular zone toward a cortical phenotype. Proc. Natl. Acad. Sci. U S A *111*, 10726–10731.

iScience, Volume *23*

Supplemental Information

Epidermal Growth Factor Receptor Inhibition Reverses Cellular and Transcriptomic Alterations Induced by Hypoxia in the Neonatal Piglet Brain

Panagiotis Kratimenos, Evan Z. Goldstein, Ioannis Koutroulis, Susan Knoblach, Beata Jablonska, Payal Banerjee, Shadi N. Malaeb, Surajit Bhattacharya, M. Isabel Almira-Suarez, Vittorio Gallo, and Maria Delivoria-Papadopoulos

Transparent Methods

Animal Experimental Procedures

Newborn Yorkshire piglets, obtained from the Willow Glenn Farm in Strasburg, PA, were used for the entire study. The animal protocol was approved by the Institutional Animal Care and Use Committee of Drexel University (IACUC protocol #200491) and the experiments with human brains were approved by the Institutional Review Board at Children's National Hospital (IRB#00011850). All methods were performed in accordance with the guidelines and regulations. A total of 10 autopsy cases of infants (5 with diagnosis of moderate or severe HX encephalopathy and 5 controls) were identified (**Supp. Table 1**).

Appropriate use of drugs was followed during experiments to eliminate pain and suffering, according to the NIH Guidelines for the Use of Laboratory Animals. A total of thirty piglets were included in the study and were placed into the following groups: NX (n=9), HX receiving vehicle (HX) (n=11), HX pre-treated with EGFR inhibitor (n=11) (EGFRi HX). [The protocol and the experimental groups are outlined in **Supp. Figure 1**. The newborn piglet model of HX has been used and studied extensively. The piglet allows for real-time monitoring of arterial blood gases, continuous blood pressure and titration of the FiO2 to achieve a precise and reproducible degree of HX, due to its large size, the presence of gyri and sulci, and the similar white/grey matter ratio and developmental age at term with human brain (Bjorkman et al., 2006; Brambrink et al., 1999; Ezzati et al., 2017; Groenendaal et al., 1999; Guerguerian et al., 2002; Haaland et al., 1997; Jain et al., 2017; Martin et al., 1997a; Martin et al., 1997b; Mehmet et al., 1998; Mehmet et al., 1994; Odden et al., 1989; Thoresen et al., 1996; Yue et al., 1997).

Anesthesia was induced with 4% Isoflurane and maintained with 0.8% Isoflurane. The piglets were intubated within 10 min of induction of anesthesia and were placed on a pressure ventilator using a mixture of 79% nitrous oxide and 21% oxygen. A peripheral IV catheter was inserted for the administration of fluids and medications. Intravenous fentanyl (10 μg/kg bolus, followed by 10μg/kg/hour continuous intravenous (IV) infusion) and pancuronium bromide (0.2 mg/kg bolus followed by 0.1μg/kg/hour continuous IV infusion) were administered. Arterial blood gases and pH were measured every 60 min through a peripheral arterial line. The physiological data of the animals used in this study are illustrated in **Supp. Table 2**.

The piglets were randomly assigned into three groups: Normoxic (NX), Hypoxic (HX) and Hypoxic pretreated with EGFR inhibitor (EGFRi HX). HX was induced by decreasing the FiO_2 to

0.06 within 5 minutes, maintained for the 60 min period and titrated to achieve a 40 % reduction in systolic BP from baseline. After 1 hour at FiO2 of 0.06, the HX piglets recovered in room air. The piglets were maintained at 38-39°C (normothermic). The EGFR inhibitor (see details below) was administered 30 minutes prior to the induction of HX. PD-168393 was the selective EGFR kinase inhibitor that was used in the study. This drug is docked into the ATP binding pocket of EGFR kinase and completely suppresses EGF-dependent receptor auto-phosphorylation, with continuous inhibition lasting as long as 8 hours in a compound-free medium (Crook et al., 2016). Using a standard recommended dosage of PD-168393, the intravenous dosage was calculated based on the formula Mass (g) = Concentration (mol/L) x Volume (L) x Molecular Weight (g/mol)(2009). The total blood volume of the newborn piglet is approximately 90ml/kg (Nowicki et al., 1985) and the suggested dose of PD-168393 in cell cultures is 10mM/ml DMSO (Xie et al., 2012). The molecular weight of PD-168393 is 369.22. The calculated dose was approximately 0.7mg/kg, and we used a slightly higher dose (1mg/kg) to ensure adequate levels of the inhibitor in the CSF.

Anesthesia was maintained throughout HX until initial recovery. Full anesthesia was also instituted prior to euthanasia and brain harvesting. The piglets were recovering for 2-4 hours in the lab extubated in room air. Only when they were able to maintain spontaneous activity and fully bear weight, they were taken back to the animal facility for 3 days until they were euthanized and the brain was harvested. The piglets were housed in groups of 2-3 piglets per cage, and environmental enrichment was provided with hanging toys, balls and deep bedding. Animals were checked 2 -3 times per day by husbandry staff and daily by veterinary staff for their health and wellbeing. The animals were randomly assigned to the study groups by blinded laboratory personnel. After the re-oxygenation period, the animals were either perfused with phosphate buffer saline (PBS) and paraformaldehyde 4% for neuropathology studies, or the brain was harvested and placed in liquid nitrogen and then stored at -80 °C for biochemical studies.

Isolation of Cerebral Cortical Cell Nuclei

Cerebral cortical nuclei were isolated according to the method of Giuffrida et al., as previously described (Giufrida et al., 1975; Kratimenos et al., 2017b). One gram of brain tissue was homogenized in 15 volumes of a medium containing 0.32M sucrose, 10mM Tris–HCl and 1mM MgCl2 (pH 6.8). The homogenate was filtered through a nylon bolting mesh (size 110μm) and

subsequently centrifuged at 850g for 10 min. The nuclei were recovered through a discontinuous gradient with a final sucrose concentration of 2.1M, which increases the yield of large neuronal nuclei. Nuclei were purified by centrifugation for 60 min at 70,000g. The nuclear pellet was collected, re-homogenized and used as nuclear preparation. The purity of neuronal nuclei was assessed by phase-contrast microscopy. Neural cell nuclei were characterized by the presence of one nucleolus per nucleus, whereas non-neural nuclei had multiple nucleoli per nucleus. The final nuclear preparation was devoid of any microsomal, mitochondrial or plasma membrane contaminant with a purity of neural nuclei of 90%. Protein content was determined by the method of Lowry et al (Lowry et al., 1951).

Measurements of ATP and Phosphocreatine Levels

Cerebral tissue HX and energy failure were confirmed by measuring the levels of high energy phosphates, ATP and PCr as previously described (Kratimenos et al., 2017a; Kratimenos et al., 2017b; Lamprecht W, 1974). Frozen cortical tissue was powdered under liquid nitrogen in 6% weight by volume perchloric acid. The extract was thawed on ice and centrifuged at 2,000g for 15 min at 4°C. The supernatant was neutralized to a pH of 7.6 using 2.23M K2CO3/0.5M triethanolamine/50mM EDTA buffer and then centrifuged at 2,000g for 15 min at 4°C. Supernatant (300μL) was added to 1 ml of buffer (50mM triethanolamine, 5mM MgCl2, 2mM EDTA, 2mM glucose, pH 7.6) and 20μL NADP. The NADP concentration was 10mg/ml in 50mM Triethanolamine (TRA)-HCl buffer. Glucose-6- phosphate dehydrogenase (10μL) was added, and the samples were incubated and read after 8 min. Hexokinase (10μL) was then added, absorbance readings were taken until a steady state was reached and ATP concentration was calculated from the increase in absorbance at 340nm. Next, ADP (20μL) and creatine kinase (20μL) were added to the solution. The samples were read every 5 min for 60 min and phosphocreatine concentrations were calculated from the increase in absorbance at 340 nm.

Measurements of CAMKIV activity

CaMKIV activity was determined as previously described by Park (Kratimenos et al., 2017b; Park and Soderling, 1995) and Soderling (Soderling, 1999) by ^{33}P incorporation (2min at 37°C) into syntide-2 in a medium containing 50mM HEPES (pH 7.5), 2mM DTT, 40μM syntide-2, 10mM Mg acetate, 5μM PKI 5–24 (protein kinase A inhibitor), 2μM PKC 19–36 (protein kinase C inhibitor), 1μM microcystin-LR (protein phosphatase 2A inhibitor), 200μM sodium orthovandate (inhibitor of ATPase, alkaline phosphatase, protein tyrosine phosphatase), 0.2mM

ATP, 1μCi ^{33}P-ATP and either 1μM calmodulin and 1mM CaCl2 (for total activity) or 1mM EGTA (for Ca^{2+}/CaM independent activity), and 10μl neuronal nuclei. Phosphorylated peptide medium (20μl) was placed on phosphocellulose P81 membranes, washed and dried. The filter was placed in 10ml of scintillation fluid and ^{33}P radioactivity counted. The difference in the presence and absence of CaM was calculated and the enzyme activity was expressed as pmol/mg of protein/min.

Neuropathology

HX injury was confirmed histologically by Hematoxylin and Eosin (H&E) stain, as previously described (Hoque et al., 2014; Kratimenos et al., 2017a; Kratimenos et al., 2017b). The evaluation of the human and piglet histology and immunohistochemistry data was performed with the evaluators totally blinded for the groups. The piglet brain was dissected and placed on ice, and areas of motor and sensory cortex, hippocampus, putamen, and caudate nucleus were dissected and fixed with formalin. The cerebellum was dissected out and the cerebral hemispheres were divided. The right cerebral hemisphere, cerebellum, and brainstem were cut into 13 coronal (5 mm each) blocks and were processed into paraffin. More specifically, upon brain removal, en bloc mid-sagittal sections comprising of the cerebrum, brainstem, and cerebellum were rapidly fixed by immersion in 4% neutral formalin, processed according to standard neurohistological procedures, and embedded in paraffin. Slides for microscopy were prepared from each block using 10μm-thick sections and stained with H&E.

Evaluation of the slides was performed by two different investigators blinded to treatment. We used a pig brain atlas to consistently identify the levels 5-6 (L5-6) on coronal sections of the cerebral cortex, the hippocampus and the putamen to complete the neuropathology scoring (Felix et al., 1999; Hoque et al., 2014). Morphological cell counting was carried out under light microscopy at 600X magnification using an oil immersion lens. Sections analyzed were typically from 2 blocks containing representative areas of the somatosensory cortex, hippocampus and putamen. In the hippocampus, cells were counted in an ocular field centered on the pyramidal layer of sector CA1 and extending into the stratum oriens and stratum radiatum. In each animal, viable neurons were counted in 8 neighboring, non-overlapping ocular fields along the CA1 region. In the putamen, viable neurons were counted in 8 ocular fields selected randomly in a raster pattern starting in the dorsolateral region of the putamen and ending in the ventral putamen. In the cortex, the hypoxic neurons, the number of viable cells and the degree of

disintegration were evaluated in each layer (I-VI) on 3 representative areas of the somatosensory cortex (cingulate and parietal).

The human brain specimens were in the form of formalin-fixed and paraffin embedded tissue blocks. Sections were obtained (10μm thickness) and slides were rehydrated with xylene and stained with H&E. Additional sections were processed for immunohistochemical staining as described in the immunohistochemistry section with phosphorylated EGFR antibody.

Normal neurons were evaluated and counted using morphological criteria. Features of ischemic injury included nuclear hyperchromasia, nuclear pyknosis, cytoplasmic eosinophilia, cytoplasmic shrinkage, cytoplasmic micro-vacuolation, and cell homogenization. Serial (10μm) adjacent sections, numbered in sequence, were used for in situ DNA end-labeling. Sections adjacent to those stained with H&E were assessed for in situ DNA fragmentation using the terminal deoxyribonucleotidyl transferase (TdT)-mediated biotin-14-dUTP nick-end labeling (TUNEL) procedure (ApopTag plus peroxidase in situ apoptosis detection kit®, Intergen, Purchase, NY). TUNEL staining was performed as described previously (Katsetos et al., 2001). The sections were deparaffinized and hydrated. Nuclei of the sections were stripped of proteins by incubation with 20 μg/ml proteinase K for 15 min at room temperature. Endogenous peroxidase was inactivated by 3% H_2O_2 for 5 min at room temperature. The sections were immersed in TDT buffer. TDT and biotinylated dUTP were diluted in TDT buffer at a concentration of 125 enzyme-units (e.u.)/ml and 12.5nmol/ml, respectively. The solution was placed on the sections, and then incubated in a moist chamber at 37°C for 60 min. The reaction was terminated by transferring the slides to TB buffer for 15 min at room temperature. The sections were covered with streptavidin peroxidase diluted 1:100 in PBS, incubated for 30 min at 37°C and stained with 3,3′-diaminobenzidine as a substrate for the peroxidase for about 30 min at 37°C. Finally, the sections were counterstained with methyl green stain.

Western Blot Analysis

Expression of the tyrosine-phosphorylated bands of CaMKIV was analyzed by Western blot, as previously described (Delivoria-Papadopoulos et al., 2011; Kratimenos et al., 2017a). Nuclear proteins were solubilized and brought to a final concentration of 1 μg/μl in a modified RIPA buffer (50mM Tris–HCl, pH 7.4, 1mM EDTA, 150mM NaCl, 1% NP-40, 0.25% sodium deoxycholate, 1mM PMSF, 1mM Na3VO4, 1mM NaF, and 1μg/ml each of aprotinin, leupeptin

and pepstatin). Five (5) µl of Laemmli buffer (100mM Tris–HCl pH 6.8, 200mM dithiothreitol, 4% SDS, 0.2% bromophenol blue, 20% glycerol) was added to every 20µg of the nuclear membrane protein mixture. The samples were heated for 5 min at 95°C. Equal protein amounts of each sample were separated by using 10% sodium dodecyl sulfate-polyacrylamide gel electrophoresis (SDS–PAGE). The proteins were electrically transferred to nitrocellulose membranes. The nitrocellulose membranes were blocked with 10% non-fat dry milk in PBS buffer for 4–6 h at 4°C. Nuclear proteins were immunoprecipitated with anti-phosphotyrosine (p-Tyr) antibody and then probed with CaMKIV antibody (sc-136249, Santa Cruz Biotech, Santa Cruz, CA) overnight at 4°C on a rocking platform. Immunoreactivity was detected by incubation with horseradish peroxidase-conjugated secondary antibody (Rockland, Gilbertsville, PA). Specific complexes were detected by enhanced chemiluminescence using the ECL detection system (Amersham Pharmacia Biotech, Buckinghamshire, UK) and analyzed by imaging densitometry (GS 700 Imaging Densitometer, Bio-Rad) using Quantity One Software (Bio-Rad). The data are expressed as optical density (OD) × mm^2.

Measurements of EGFR Kinase Activity

The assay was performed according to Alessi et al. by ^{33}P incorporation into an EGFR-specific peptide substrate for 30 min at 30°C in a 40µl medium containing the prepared membranes, assay buffer [250 mM Tris-HCl buffer (pH 7.0), 1mM EDTA (Ethylene diamine tetraacetic acid), 0.1% Tween-20, 125mM Magnesium chloride, 25mM Manganese chloride, 2mM DTT (Dithiothreitol), and 2mM EGTA (Ethylene glycol tetra-acetic acid)], 300µM EGFR-kinase peptide substrate [(KVEKIGEGTYGVVYK) corresponding to amino acids 6-20 of p34cdc2], and 50µM P^{33}-ATP (0.5µCi).(Alessi et al., 1995) The reaction was halted by 10µl 40% TCA (Trichloroacetic acid). The reaction mixture was then pelleted and 30µl supernatant spotted on P81 phosphocellulose paper, washed 3 times with 0.75% phosphoric acid and dried for a minimum of 30 minutes. Radioactivity was counted by liquid scintillation. The data provided for EGFR kinase activity are expressed as pmoles/mg protein/hr.

Immunohistochemistry and cell counting

Immunohistochemistry was performed on formalin fixed and deparaffinized sections, which were blocked for 1 hour in a solution containing PBST (0.1% TritonX-100) and 20% normal goat serum (NGS), followed by overnight incubation at 4°C in primary antibodies diluted in PBST and 5% NGS. Primary antibody dilutions were 1:500 rabbit anti-GFAP (Abcam), and 1:250 for rabbit anti-Olig2 (Millipore), 1:1000 rabbit anti-Ki67 (Abcam), and mouse anti-NeuN (Calbiochem),

rabbit anti-cleaved Caspase-3 (Cell Signaling). Sections were incubated with species appropriate secondary antibodies (Jackson Immunoresearch; 1:500) for 2h at room temperature. Sections were treated with 4', 6-diamidino-2-phenylindole (DAPI) for 10-15 min and mounted with Mowiol.

Image acquisition and analysis

We used a confocal LSM (Zeiss 510) microscope using 40x oil objectives to image the cortical tissue. Z-stack images of 1µm thick single planes were captured using Zeiss software. Four different lasers were used to image localization of FITC (488 nm excitation), CY3 (580 nm excitation), CY5 (647 nm excitation), and DAPI (400 nm excitation). A Zeiss ApoTome.2 microscope was also used for optical sectioning of the L5 and L6 sagittal sections of brain tissue. The images were acquired using Plan-NeoFluar40x/1.03 oil objective. The Colibri 7 Type RGB-UV light source equipped with four solid state LED lines 385nm, 475nm, 555nm and 630nm were used to excite the fluorochromes and the fluorescence was collected on to the Axiocam 503 monochromatic camera through filter Set 90 HE (Excitation filters BP 385/30, BP 469/38, BP555/30, BP 631/33; QBS 405+493+575+653; Emission filters QBP 425/30). ZEN 2.3 (blue edition) software was used to acquire the images.

Images were viewed using NIH ImageJ and the Zeiss LSM Image Browser. All histological quantifications were performed in a blinded manner. Immunolabeled cells were manually counted in each optical section using the ImageJ "Cell Counter" plugin. An average of three images was taken for each somatosensory cortical section. For each image, the total number of cells was counted and normalized to volume.

RNA sequencing and bioinformatics

Total RNA was isolated with an RNAeasy Tissue isolation kit (Qiagen), that included the DNase incubation step to remove DNA contamination. RNA was quantified with a Qubit fluorometer (Thermofisher) and quality was determined on a bioanalyzer (Pico Chip, Agilent). Paired-end libraries were prepared from 1 ug RNA (RIN>8) using the TruSeq Stranded mRNA Library

Preparation Kit (Illumina), according to the manufacturer's protocol. Adapter-dimers were removed using AMPure XP beads and the libraries sequenced on a NovaSeq S1 100 cycle Xp2 Flow cell (2x50 bp) (Illumina) at the Johns Hopkins University Genome Sciences and Bioinformatics core.

The quality of raw fastq reads was evaluated with FastQC version 0.11.5 (Wingett and Andrews, 2018). All samples had more than 19M reads (average of 26M). STAR 2.5.3a (Dobin et al., 2013) was used to map the reads to the reference Pig genome (Sscrofa11.1) (Schook et al., 2005). Most of the samples had an alignment rate > 85%. Mapped reads were counted using featureCounts (subread version 1.6.2)(Liao et al., 2014) with a reference genomic feature file (Gene transfer format- GTF). Overall summary reports were analyzed using MultiQC v1.6 (Ewels et al., 2016) Differential gene expression (DGE) analysis was performed using default parameters with Deseq2 version 1.26 (R 3.6) (Love et al., 2014). Groups were compared using the Wald test with Benjamini-Hochberg correction (adjusted $p < 0.05$). Reported DEGS have normalized read counts above 5 in all samples. Gprofiler, GPLOT and Ingenuity Pathway Analysis (Qiagen) were used to identify and graph cellular and molecular functions.

RT-PCR

RNA-seq data were validated with Taqman qRT-PCR (ThermoFisher Scientific, Waltham, MA). Total RNA (200 ng) was converted into cDNA using a High Capacity cDNA Reverse Transcription Kit. (ThermoFisher Scientific, Waltham, MA). RT-PCR was performed on 9 samples, run in triplicate (3 NX controls, 3 HX and 3 EGRFRi HX) using the 384 well Taqman protocol: 12 ul total reaction=6ul of Taqman FAST advanced mastermix, 0.6 ul control probe and 0.6 ul of gene of interest. RT-PCR was performed on a QuantStudio 7 instrument (Thermo Fisher Scientific). Ct values were averaged for each of the triplicates and normalized to the control. The delta-delta Ct method was used to calculate the relative fold expression. The following probes were used for expression of genes of interest: 1) BDNF (Ss03822335_s1), 2)CAMK2A (ARXGTX3), 3) CAMKK2 (Ss06875600_m1), 4) DRD1 (Ss03387703_u1), 5) DRD2 (Ss04326684_m1), 6) FEZF2 (ARYMMJC), 7) CREB5 (AR7DTEX), and 1 control gene PGK1 (Ss03389150_m1). Probe information is in **Supp. Table 3.**

Statistical analysis

Statistical analysis of the data on ATP, PCr, EGFR, and CaMKIV enzyme activity, and CAMKIV expression, and neuropathology was performed using a one-way analysis of variance (ANOVA). Specific numbers of animals are denoted in each figure legend. Prior to statistical testing, the D'Agostino & Pearson normality test was used to show that our data was normally distributed. Significance was calculated using GraphPad (v.8.3.0, San Diego, CA). All data are presented as averages ± SD. All cell counting, enzyme activity and western blot data were statistically compared using one-way ANOVA to determine whether overall differences exist across study groups at specific ages. Comparisons between groups were treated as unplanned comparisons, which were adjusted using a Tukey's correction. A two-tailed type 1 error (p-value < 0.05) was used to determine statistical significance. The degree of statistical significance was denoted using asterisks (* p < 0.05; ** p < 0.01; *** p < 0.005). Where relevant, exact p values are provided. Neuropathology scoring (ordinal data) was reported as medians ± Interquartile range (IQR).

Human data analysis and Power calculation: With 40% difference, 30% standard deviation, 5% error in morphological characteristics of cerebellar neurons between control and patients per age group, 10 patients gave 85% of power per each condition. We included 5 infants/group, thus a total of 10 patients. Each infant has two separate data sets (H&E and EGFR staining), and thus a total of 10 data points/case in each age group.

Supplemental Items:

Supplemental Figure 1. HX induces EGFR activation and changes in biochemical energetics in piglet cortex. (**a**) Schematic representation of the experimental outline**.** (**b**) Enzymatic activity of the phosphorylated EGFR in the piglet cortex was significantly increased following HX. EGFR blockade totally reversed the HX-induced increased activation of EGFR in the piglet cortex (n=4/group). (**c** and **d**) Both ATP and PCr levels were significantly reduced in all HX groups, as compared to the normoxic (NX) groups. No significant difference in cerebral tissue high energy compounds was found in the HX groups with and without EGFRi, indicating that similar levels of HX were achieved in both groups. Pretreatment with EGFRi did not reverse the energy failure due to HX. ATP: adenosine triphosphate, PCr: Phosphocreatine, NX: Normoxic (n=4), HX: Hypoxic, EGFRi HX: Epidermal growth factor receptor blockade and HX (n=4). Data are represented as mean +/- SD, one-way ANOVA, * p<0.05, *** p<0.001, Related to **Figure 1-7**

Supplemental Figure 2. EGFR blockade reverses the effects of HX on CaMKIV activation. (**a** and **b**) Expression (n=3/group) (**a**) and enzymatic activity (n=5/group) (**b**) of CAMKIV in the piglet cortex was significantly increased following HX. EGFR blockade prior to HX significantly reduced the expression and activity of CAMKIV in the piglet cortex. NX: Normoxic, HX: Hypoxic, EGFRi HX: Epidermal growth factor blockade and HX, CaMKIV: calcium/calmodulin-dependent protein kinase type IV. Data are represented as mean +/- SD, one-way ANOVA, * $p<0.05$, ** $p<0.01$, Related to **Figure 7**

Supplemental Figure 3. (**a-g**) RNA sequencing validation using qPCR for significantly differentially expressed genes that are involved in EGFR signaling. In alignment with the transcriptomic data, HX altered the expression of *CAMKK2A* (**a**)*, CAMK2A* (**b**)*, DRD1* (**c**)*, DRD2* (**d**) *and FEZF2* (**e**)*, CREB5* (**f**) *and BDNF* (**g**), while EGFR blockade normalized it (**a-g**). NX: Normoxic, HX: Hypoxic, EGFRi HX: Epidermal growth factor blockade and HX. CAMK2A: Calcium/Calmodulin Dependent Protein Kinase II Alpha, CAMKK2: Calcium/Calmodulin Dependent Protein Kinase Kinase 2, DRD1: Dopamine receptor D_1, DRD2: Dopamine receptor D_2, FEZF2: FEZ Family Zinc Finger 2, CREB5: Cyclic AMP-responsive element-binding protein 5, BDNF: Brain-derived neurotrophic factor. Data are represented as mean +/- SD, one-way ANOVA, * p<0.05, Related to **Figure 5-7**

Table S1. Demographic and clinical characteristics of the patients included in the study. HIE: hypoxic ischemic encephalopathy, HT: therapeutic hypothermia protocol, PMI: postmortem interval, SIDS: sudden infant death syndrome, N/A: non-applicable, Related to **Figure 1**

Table S2. Physiologic parameters for piglets including the maximum reduction from baseline systolic blood pressure (SBP) and arterial partial pressure of oxygen (PaO2) and carbon dioxide (PCO2). HX: Hypoxia, NX: normoxia, EGFRi HX: Hypoxia followed by administration of EGFR inhibitor. SBP = systolic blood pressure; Pre = measurement was obtained before the HX; Post = measurement was obtained 1 h after the HX; PCO_2 = Partial pressure of carbon dioxide in arterial blood (mmHg). PaO_2 = Partial pressure of oxygen in arterial blood (mmHg) Related to **Figure 2-7**

Table S3. Assay IDs and Sequence of TAQMAN Probes Utilized for RT-PCR. Probes were supplied by Life Technologies (Carlsbad, CA), Related to Figure, Related to **Figure 5-7**

REFERENCES

(2009). Compendium of polymer terminology and nomenclature: IUPAC recommendations, 2008. Choice: Current Reviews for Academic Libraries *47*, 141-141.

Alessi, D.R., Cohen, P., Ashworth, A., Cowley, S., Leevers, S.J., and Marshall, C.J. (1995). Assay and expression of mitogen-activated protein kinase, MAP kinase kinase, and Raf. Methods Enzymol *255*, 279-290.

Bjorkman, S.T., Foster, K.A., O'Driscoll S, M., Healy, G.N., Lingwood, B.E., Burke, C., and Colditz, P.B. (2006). Hypoxic/Ischemic models in newborn piglet: comparison of constant FiO2 versus variable FiO2 delivery. Brain Res *1100*, 110-117.

Brambrink, A.M., Martin, L.J., Hanley, D.F., Becker, K.J., Koehler, R.C., and Traystman, R.J. (1999). Effects of the AMPA receptor antagonist NBQX on outcome of newborn pigs after asphyxic cardiac arrest. J Cereb Blood Flow Metab *19*, 927-938.

Crook, M., Upadhyay, A., Ido, L.J., and Hanna-Rose, W. (2016). EGFR Cell Survival Signaling Requires Phosphatidylcholine Biosynthesis. G3 (Bethesda).

Delivoria-Papadopoulos, M., Ashraf, Q.M., and Mishra, O.P. (2011). Mechanism of CaM kinase IV activation during hypoxia in neuronal nuclei of the cerebral cortex of newborn piglets: the role of Src kinase. Neurochem Res *36*, 1512-1519.

Dobin, A., Davis, C.A., Schlesinger, F., Drenkow, J., Zaleski, C., Jha, S., Batut, P., Chaisson, M., and Gingeras, T.R. (2013). STAR: ultrafast universal RNA-seq aligner. Bioinformatics *29*, 15-21.

Ewels, P., Magnusson, M., Lundin, S., and Kaller, M. (2016). MultiQC: summarize analysis results for multiple tools and samples in a single report. Bioinformatics *32*, 3047-3048.

Ezzati, M., Kawano, G., Rocha-Ferreira, E., Alonso-Alconada, D., Hassell, J.K., Broad, K.D., Fierens, I., Fleiss, B., Bainbridge, A., Price, D.L.*, et al.* (2017). Dexmedetomidine Combined with Therapeutic Hypothermia Is Associated with Cardiovascular Instability and Neurotoxicity in a Piglet Model of Perinatal Asphyxia. Dev Neurosci *39*, 156-170.

Felix, B., Leger, M.E., Albe-Fessard, D., Marcilloux, J.C., Rampin, O., and Laplace, J.P. (1999). Stereotaxic atlas of the pig brain. Brain Res Bull *49*, 1-137.

Giufrida, A.M., Cox, D., and Mathias, A.P. (1975). RNA polymerade activity in various classes of nuclei from different regions of rat brain during postnatal development. J Neurochem *24*, 749-755.

Groenendaal, F., de Graaf, R.A., van Vliet, G., and Nicolay, K. (1999). Effects of hypoxia-ischemia and inhibition of nitric oxide synthase on cerebral energy metabolism in newborn piglets. Pediatr Res *45*, 827-833.

Guerguerian, A.M., Brambrink, A.M., Traystman, R.J., Huganir, R.L., and Martin, L.J. (2002). Altered expression and phosphorylation of N-methyl-D-aspartate receptors in piglet striatum after hypoxia-ischemia. Brain Res Mol Brain Res *104*, 66-80.

Haaland, K., Loberg, E.M., Steen, P.A., and Thoresen, M. (1997). Posthypoxic hypothermia in newborn piglets. Pediatr Res *41*, 505-512.

Hoque, N., Sabir, H., Maes, E., Bishop, S., and Thoresen, M. (2014). Validation of a neuropathology score using quantitative methods to evaluate brain injury in a pig model of hypoxia ischaemia. J Neurosci Methods *230*, 30-36.

Jain, A., Kratimenos, P., Koutroulis, I., Jain, A., Buddhavarapu, A., and Ara, J. (2017). Effect of Intranasally Delivered rh-VEGF165 on Angiogenesis Following Cerebral Hypoxia-Ischemia in the Cerebral Cortex of Newborn Piglets. Int J Mol Sci *18*.

Katsetos, C.D., Spandou, E., Legido, A., Taylor, M.L., Zanelli, S.A., de Chadarevian, J.P., Christakos, S., Mishra, O.P., and Delivoria-Papadopoulos, M. (2001). Acute hypoxia-induced alterations of calbindin-D28k immunoreactivity in cerebellar Purkinje cells of the guinea pig fetus at term. J Neuropathol Exp Neurol *60*, 470-482.

Kratimenos, P., Koutroulis, I., Agarwal, B., Theocharis, S., and Delivoria-Papadopoulos, M. (2017a). Effect of Src Kinase inhibition on Cytochrome c, Smac/DIABLO and Apoptosis Inducing Factor (AIF) Following Cerebral Hypoxia-Ischemia in Newborn Piglets. Sci Rep *7*, 16664.
Kratimenos, P., Koutroulis, I., Jain, A., Malaeb, S., and Delivoria-Papadopoulos, M. (2017b). Effect of Concurrent Src Kinase Inhibition with Short-Duration Hypothermia on Ca2+/Calmodulin Kinase IV Activity and Neuropathology after Hypoxia-Ischemia in the Newborn Swine Brain. Neonatology *113*, 37-43.
Lamprecht W, S.P., Heinz F, Weissner H. (1974). Methods of Enzymatic Analysis, In: Creatine phosphate. , Vol 4.
Liao, Y., Smyth, G.K., and Shi, W. (2014). featureCounts: an efficient general purpose program for assigning sequence reads to genomic features. Bioinformatics *30*, 923-930.
Love, M.I., Huber, W., and Anders, S. (2014). Moderated estimation of fold change and dispersion for RNA-seq data with DESeq2. Genome Biol *15*, 550.
Lowry, O.H., Rosebrough, N.J., Farr, A.L., and Randall, R.J. (1951). Protein measurement with the Folin phenol reagent. J Biol Chem *193*, 265-275.
Martin, L.J., Brambrink, A., Koehler, R.C., and Traystman, R.J. (1997a). Primary sensory and forebrain motor systems in the newborn brain are preferentially damaged by hypoxia-ischemia. J Comp Neurol *377*, 262-285.
Martin, L.J., Brambrink, A.M., Lehmann, C., Portera-Cailliau, C., Koehler, R., Rothstein, J., and Traystman, R.J. (1997b). Hypoxia-ischemia causes abnormalities in glutamate transporters and death of astroglia and neurons in newborn striatum. Ann Neurol *42*, 335-348.
Mehmet, H., Yue, X., Penrice, J., Cady, E., Wyatt, J.C., Sarraf, C., Squier, M., and Edwards, A.D. (1998). Relation of impaired energy metabolism to apoptosis and necrosis following transient cerebral hypoxia-ischaemia. Cell Death Differ *5*, 321-329.
Mehmet, H., Yue, X., Squier, M.V., Lorek, A., Cady, E., Penrice, J., Sarraf, C., Wylezinska, M., Kirkbride, V., Cooper, C.*, et al.* (1994). Increased apoptosis in the cingulate sulcus of newborn piglets following transient hypoxia-ischaemia is related to the degree of high energy phosphate depletion during the insult. Neurosci Lett *181*, 121-125.
Nowicki, P.T., Hansen, N.B., Stonestreet, B.S., Yao, A.C., and Oh, W. (1985). The effect of blood volume expansion on gastrointestinal oxygenation in piglets. Pediatr Res *19*, 268-271.
Odden, J.P., Stiris, T., Hansen, T.W., and Bratlid, D. (1989). Cerebral blood flow during experimental hypoxaemia and ischaemia in the newborn piglet. Acta Paediatr Scand Suppl *360*, 13-19.
Park, I.K., and Soderling, T.R. (1995). Activation of Ca2+/calmodulin-dependent protein kinase (CaM-kinase) IV by CaM-kinase kinase in Jurkat T lymphocytes. J Biol Chem *270*, 30464-30469.
Schook, L.B., Beever, J.E., Rogers, J., Humphray, S., Archibald, A., Chardon, P., Milan, D., Rohrer, G., and Eversole, K. (2005). Swine Genome Sequencing Consortium (SGSC): a strategic roadmap for sequencing the pig genome. Comp Funct Genomics *6*, 251-255.
Soderling, T.R. (1999). The Ca-calmodulin-dependent protein kinase cascade. Trends Biochem Sci *24*, 232-236.
Thoresen, M., Haaland, K., Loberg, E.M., Whitelaw, A., Apricena, F., Hanko, E., and Steen, P.A. (1996). A piglet survival model of posthypoxic encephalopathy. Pediatr Res *40*, 738-748.
Wingett, S.W., and Andrews, S. (2018). FastQ Screen: A tool for multi-genome mapping and quality control. F1000Res *7*, 1338.
Xie, G., Peng, Z., and Raufman, J.P. (2012). Src-mediated aryl hydrocarbon and epidermal growth factor receptor cross talk stimulates colon cancer cell proliferation. Am J Physiol Gastrointest Liver Physiol *302*, G1006-1015.

Yue, X., Mehmet, H., Penrice, J., Cooper, C., Cady, E., Wyatt, J.S., Reynolds, E.O., Edwards, A.D., and Squier, M.V. (1997). Apoptosis and necrosis in the newborn piglet brain following transient cerebral hypoxia-ischaemia. Neuropathol Appl Neurobiol *23*, 16-25.

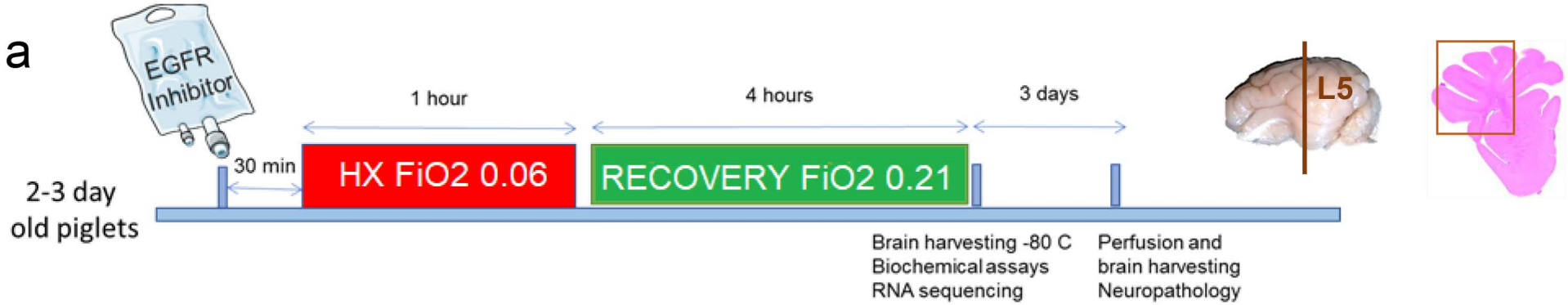

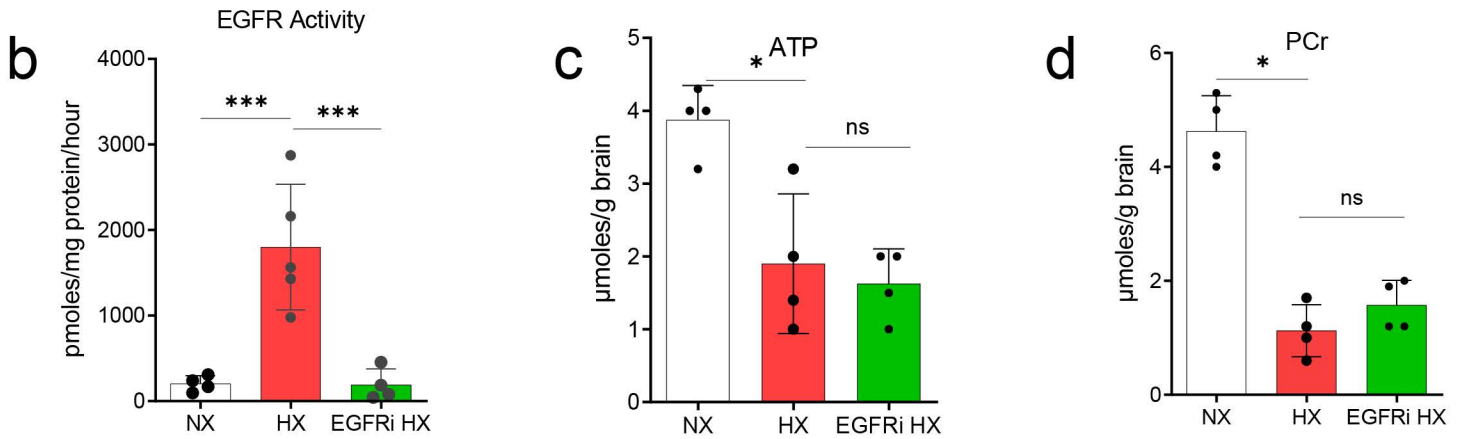

Supp. Figure 1

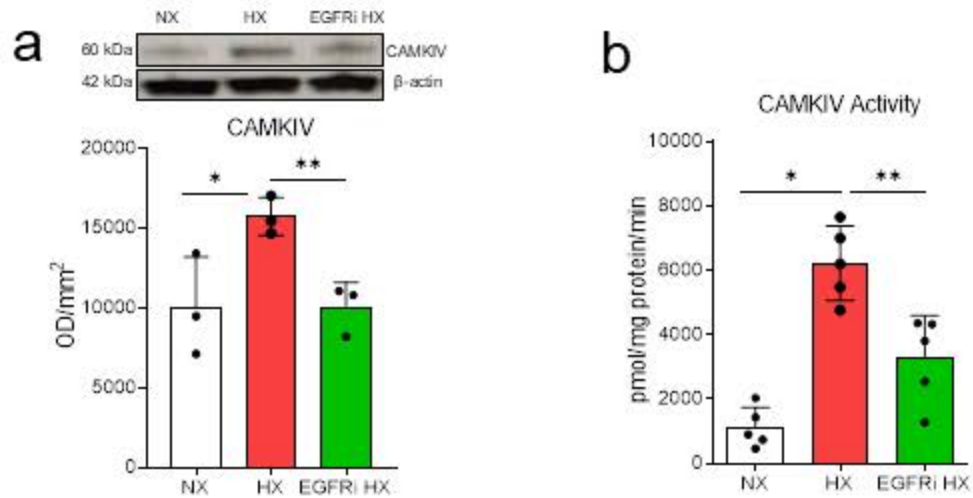

Supp. Figure 2

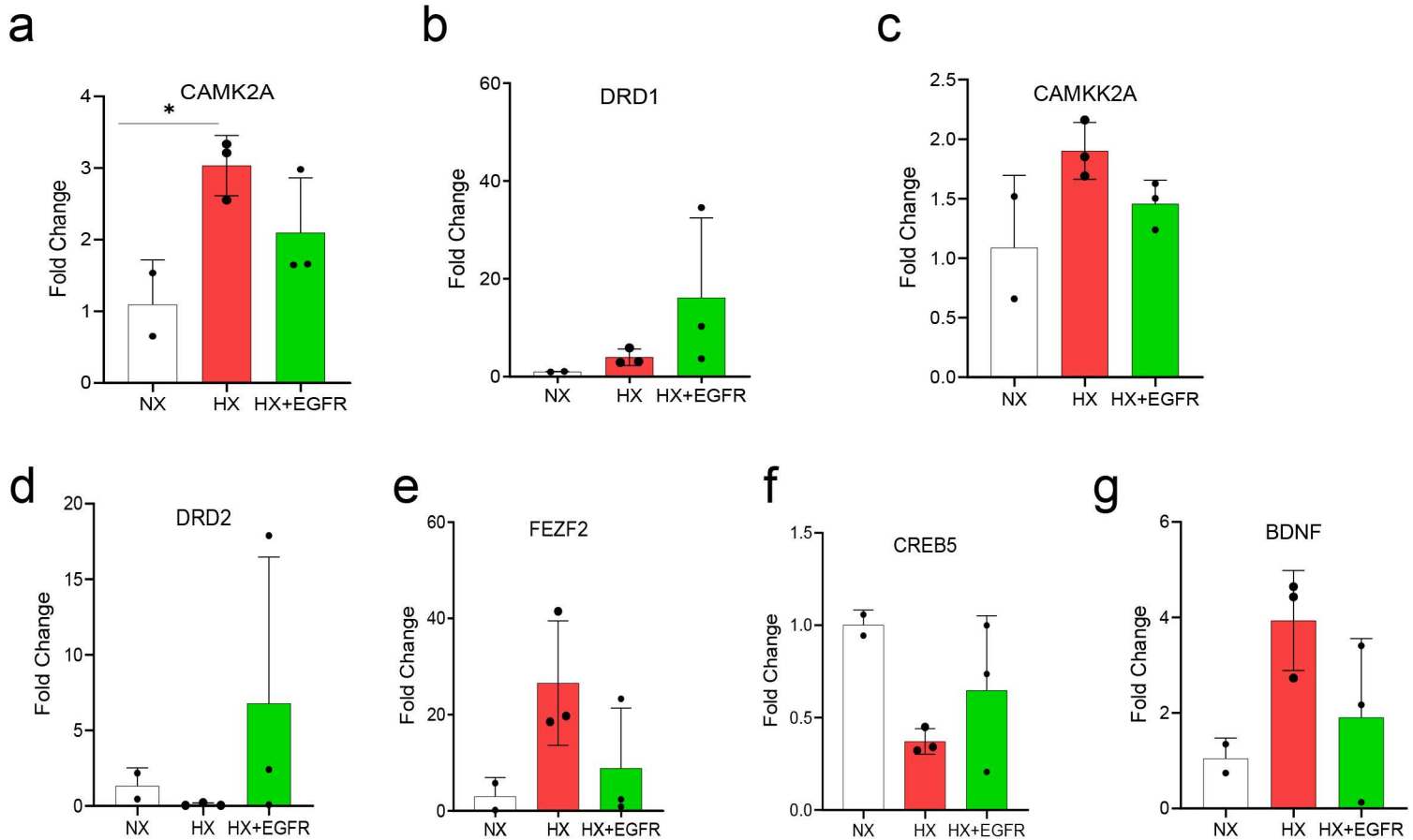

Supp. Figure 3

Table S1

Subject	GA	APGAR score	PMI (hours)	pH/ Base deficit	Age at death (days)	Brain mass (gr)	Cause of death	Reason for no HT
1.	34 5/7	1,3,3	24	7.13/-4	20	270.3	Severe HIE	Preterm infant – not eligible for HT
2.	38 4/7	8,8	48	7.03/-12	90	277.4	Cardiac failure due to Hypoplastic left heart syndrome	Cardiac disease – not eligible for HT
3.	38 6/7	0,2,3	24	7.19/-7.2	2	481	Severe HIE	Subacute HIE – only 4 hours of HT –then rewarmed
4.	40	1,2,3	12	-	5	408	Severe HIE	>6 hours old on diagnosis – not eligible for HT
5.	40 5/7	1,3,3	24	-	4	440	Severe HIE, tight nuchal cord	Rewarmed due to redirection of care
6.	40	-	36	-	63	550	SIDS	N/A
7.	40	9, 9	11	-	179	930	SIDS, Asphyxiation	N/A
8.	39	-	46	-	146	720	SIDS, co-sleeping	N/A
9.	40	9,9	53	-	147	696	SIDS, co-sleeping	N/A
10.	40	-	27	-	236	783	SIDS, asphyxiation	N/A

Table S1: Demographic and clinical characteristics of the patients included in the study. HIE: hypoxic ischemic encephalopathy, HT: therapeutic hypothermia protocol, PMI: postmortem interval, SIDS: sudden infant death syndrome, N/A: non-applicable

Characteristic	NX (n = 9)	HX (n = 11)	EGFRi HX (n = 11)
Male	4	5	4
Female	4	6	7
Weight (kg)	2.6 (0.6)	1.8 (0.43)	1.9 (0.5)
Temperature (°C)	38.2 (0.5)	38.6 (0.37)	38.7 (0.2)
Maximum Reduction from Baseline SBP (%±SE)	11±6	32±4	21±8
pH pre	7.44 (0.0323)	7.45 (0.055)	7.45 (0.067)
pH post	7.45 (0.0723)	7.31 (0.067)	7.21 (0.022)
PCO_2 post	37 (2.1)	38.7 (4.22)	36 (3.5)
PaO_2 post	81.4 (2.765)	22.4 (4.3)	19.7 (2)

Table S2. Physiologic parameters for piglets including the maximum reduction from baseline systolic blood pressure (SBP) and arterial partial pressure of oxygen (PaO2) and carbon dioxide (PCO2). HX: Hypoxia, NX: normoxia, EGFRi HX: Hypoxia followed by administration of EGFR inhibitor. SBP = systolic blood pressure; Pre = measurement was obtained before the HX; Post = measurement was obtained 1 h after the HX; PCO_2 = Partial pressure of carbon dioxide in arterial blood (mmHg). PaO_2 = Partial pressure of oxygen in arterial blood (mmHg)

Table S3

Assay ID	Assay Name	Context Sequence
AR7DTEX	CREB5	GGCAACCAAGCACAGGTCTCACCAG
ARXGTX3	CAMK2A	CCCCAACATTGTCCGGCTTCATGAC
ARYMMJC	FEZF2	ATTATCCACACGCAGGAAAAGCCGC
Ss03387703_u1	DRD1	GAAGGAAGAGGCAGGTGGCATAGCA
Ss04326684_m1	DRD2	CCATTGTTCTCGGCGTGTTCATCAT
Ss06875600_m1	CAMKK2	ATCTGTACATGGTGTTTGAACTGGT
Ss03822335_s1	BDNF	AAAAGACGGCAGTGGACATGTCGGG
Ss03389150_m1	PGK1	TAGAGCTCCTGGAAGGTAAAGTCCT

Table S3. Assay IDs and Sequence of TAQMAN Probes Utilized for RT-PCR. Probes were supplied by Life Technologies (Carlsbad, CA).